Damage Detection in Blade-Stiffened Anisotropic Composite Panels Using Lamb

Wave Mode Conversions

by

Anthony James Vizzini, II

A Thesis Presented in Partial Fulfillment
of the Requirements for the Degree
Master of Science

Approved April 2012 by the
Graduate Supervisory Committee

Aditi Chattopadhyay, Chair
Antonia Papandreou-Suppappola
Masoud Yekani Fard

ARIZONA STATE UNIVERSITY

MAY 2012

ABSTRACT

Composite materials are increasingly being used in aircraft, automobiles, and other applications due to their high strength to weight and stiffness to weight ratios. However, the presence of damage, such as delamination or matrix cracks, can significantly compromise the performance of these materials and result in premature failure. Structural components are often manually inspected to detect the presence of damage. This technique, known as schedule based maintenance, however, is expensive, time-consuming, and often limited to easily accessible structural elements. Therefore, there is an increased demand for robust and efficient Structural Health Monitoring (SHM) techniques that can be used for Condition Based Monitoring, which is the method in which structural components are inspected based upon damage metrics as opposed to flight hours. SHM relies on *in situ* frameworks for detecting early signs of damage in exposed and unexposed structural elements, offering not only reduced number of schedule based inspections, but also providing better useful life estimates. SHM frameworks require the development of different sensing technologies, algorithms, and procedures to detect, localize, quantify, characterize, as well as assess overall damage in aerospace structures so that strong estimations in the remaining useful life can be determined. The use of piezoelectric transducers along with guided Lamb waves is a method that has received considerable attention due to the weight, cost, and function of the systems based on these elements.

The research in this thesis investigates the ability of Lamb waves to detect damage in feature dense anisotropic composite panels. Most current research negates the effects of experimental variability by performing tests on structurally simple isotropic plates that are used as a baseline and damaged specimen. However, in actual applications, variability cannot be negated, and therefore there is a need to research the effects of complex sample geometries, environmental operating conditions, and the effects of variability in material properties.

This research is based on experiments conducted on a single blade-stiffened anisotropic composite panel that localizes delamination damage caused by impact. The overall goal was to utilize a correlative approach that used only the damage feature produced by the delamination as the damage index. This approach was adopted because it offered a simplistic way to determine the existence and location of damage without having to conduct a more complex wave propagation analysis or having to take into account the geometric complexities of the test specimen. Results showed that even in a complex structure, if the damage feature can be extracted and measured, then an appropriate damage index can be associated to it and the location of the damage can be inferred using a dense sensor array.

The second experiment presented in this research studies the effects of temperature on damage detection when using one test specimen for a benchmark data set and another for damage data collection. This expands the previous experiment into exploring not only the effects of variable temperature, but also the effects of high experimental variability. Results from this work show that the

damage feature in the data is not only extractable at higher temperatures, but that the data from one panel at one temperature can be directly compared to another panel at another temperature for baseline comparison due to linearity of the collected data.

DEDICATION

To George Lucas, for teaching me to dream

To Legos, for teaching me to build

To my mother and father, for teaching me to succeed

And to all others who believed in me, pushed me, and pulled me along the way.

Thank you.

ACKNOWLEDGEMENTS

TABLE OF CONTENTS

LIST OF TABLES

LIST OF FIGURES

CHAPTER 1

INTRODUCTION

In today's aerospace and automotive industries, composite materials are becoming ever more present in structural applications due to their high strength to weight and stiffness to weight ratios. However, the presence of damage, such as delamination or matrix cracks, can compromise their performance significantly and result in premature failure. Current industry methods used to perform detection of this type of damage require the use of nondestructive evaluation (NDE) approaches for Schedule Based Monitoring (SBM) such as acoustic emission [1], flash thermography [2], eddy current method [3], and ultrasonic scanning [4]. These methods often require the inspected structure to not only be taken out of service, but in some cases disassembled. Some elements, such as ribs or spars, need specialized ports in the wing for access. This adds weight to the overall structure because the weakening caused by the ports requires additional supporting structural elements. Therefore, there is an increased demand for robust and efficient Structural Health Monitoring (SHM) techniques so that the industry can shift from SBM to Condition Based Monitoring (CBM), allowing for extensive reduction in the time the aircraft is out of service, and thus reducing overall maintenance and opportunity costs. This shift will not only help reduce the number of schedule based inspections, but will also provide better useful life estimates.

The development of robust SHM techniques will enable the aerospace industry to monitor a component at all times and assess its structural integrity,

while predicting time at which the component needs to be repaired and/or replaced. The objective of SHM is to detect damage *before* it reaches a critical state and improve the safety and trustworthiness of structures [5]. Therefore, it is critical that accurate detection models [6], sensor optimization models [7], and statistical models of SHM techniques be developed for damage classification of a given structure [8].

A robust SHM framework requires the installation of a distributed sensor network so that damage measurements can be made rapidly and frequently without significant effort or expense. Several sensor networks, including strain gauges [9], piezoelectric transducers [10], macro fiber composite (MFC) sensors [11], and fiber optic sensors [12] have been investigated in current literature for this purpose. Both active and passive detection techniques have also been proposed with success in both metallic and composite structures using these sensor networks. Wave based techniques work very well for detection and localization of damage in metals [13, 14]. In composite structures, however, the use of wave based techniques poses substantial obstacles. The waves that get reflected by damage, boundaries, and geometric features are direction dependent due to the inherent anisotropy of the system. As a result, changes in wave signature that have resulted from damage alone are difficult to isolate, making detection in composites a more challenging task than detection in metals. The difficulty level further increases when the composite sample is highly anisotropic and feature dense due to further scattering, attenuation, and dispersion of the waves [15].

The use of Lamb waves and piezoelectric sensors, such as lead zirconate titanate (PZT), allow for an active approach for *in situ* damage detection in composites. By using the PZTs as both actuator and sensor, a round robin approach can be utilized to collect a breadth of data for damage detection. PZTs are popular because they can be easily mounted on surfaces and are relatively inexpensive. PZTs operate by converting supplied electrical energy into mechanical energy. When a current is supplied to a PZT, it vibrates the PZT at very high frequencies. The high frequency vibration of the PZT results in a transfer of the mechanical load back to a readable electrical current. Guided waves are waves that can be produced in thin plates, beams, and shell structures using PZTs. Lamb waves, the guided waves used in this research, can travel over long distances, even in composite materials which have a high attenuation ratio [16].

This chapter provides an overview of Lamb waves, their advantages, and their use as a sensing method for SHM. In addition, research being conducted on damage detection and localization in composites performed using PZT sensors and Lamb waves are also discussed. The chapter concludes with a presentation on the overall objectives of this work.

1.1   Lamb Wave Sensing

Lamb waves, discovered in 1917 by Horace Lamb, exist in thin plate-like structures such as panels, plates, and small beams with parallel free boundaries [16]. Mindlin [17] was the first to develop a comprehensive plate theory in

parallel with work conducted by Schoch and Frederick between the mid-1950s and 1960s [18]. In 1961, Worlton [19] introduced Lamb waves as a means of damage detection. These works taken together established the utilization of Lamb waves today for non-destructive evaluation (NDE).

Lamb waves are useful for NDE functions for several reasons: They can travel long distances, even in high attenuation materials such as composites. They have a high susceptibility to interference along and around the propagation path [16], as a result of which large areas, such as a composite wing skin of an aircraft can be interrogated with ease. Lamb waves are also able to detect not just surface damage, but also internal damage because the entire thickness of the material can be interrogated using a variety of Lamb wave modes. Overall, Lamb wave based damage detection methods can be used to (1) inspect large structures without disturbing coating or insulation on the inspected structure; (2) inspect 100% of the cross-sectional area of a structure over a reasonably long length; (3) remove the need for expensive structural probing; (4) detect multiple defects; and (5) perform with very low energy and cost [16]. Using data collected from the Lamb wave interrogations, inferences can be made to the presence, location, and severity of the damage. From this information, accurate useful life estimations can also be determined.

1.1.1 Lamb wave principles

Lamb waves are made up of a combination of longitudinal modes and shear modes. Their propagation characteristics vary with angle, excitation

frequency, and the structural geometry of the material; they can be symmetric, S_0, or anti-symmetric, A_0 (Figure 1).

Symmetric Lamb wave mode

Anti-symmetric Lamb wave mode
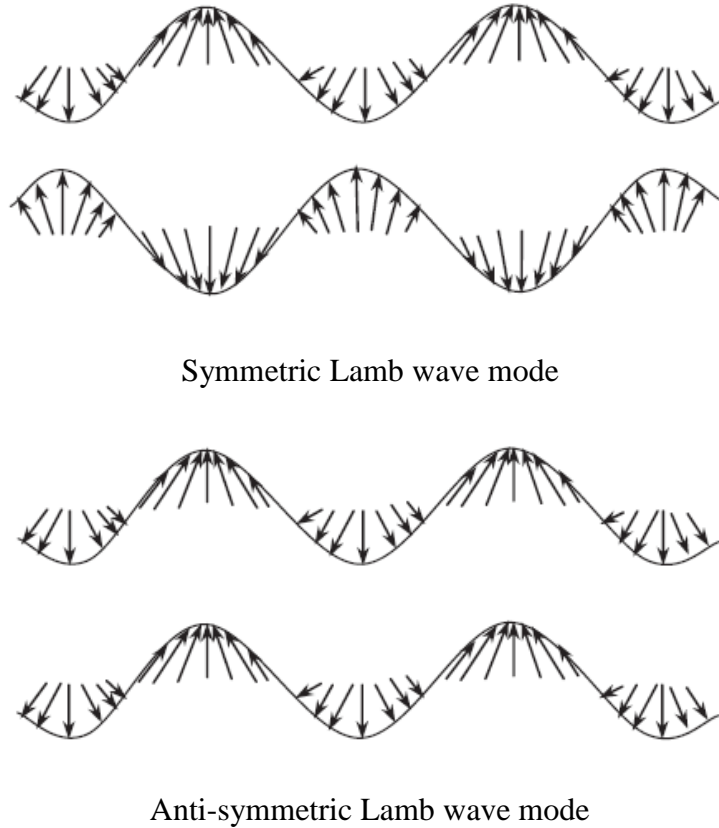
Figure 1. Symmetric and anti-symmetric Lamb wave modes [16]

Equation 1a and 1b show the formulation of Lamb waves [20] where h, k, c_L, c_T, ω are the plate thickness, wavenumber, longitudinal and transverse mode velocity, phase velocity, and wave circular frequency, respectively. Equation 1 shows that propagation velocity is dependent on frequency; this is called dispersion.

$$\frac{\tan(qh)}{\tan(ph)} = \frac{-4k^2\,qp}{(k^2 - q^2)^2} \quad \text{for symmetric modes} \qquad \text{1a)}$$

$$\frac{\tan(qh)}{\tan(ph)} = \frac{(k^2 - q^2)^2}{4k^2qp} \quad \text{for anti-symmetric modes} \qquad \text{1b)}$$

$$p^2 = \frac{\omega^2}{c_L^2} - k^2, \qquad q^2 = \frac{\omega^2}{c_T^2} - k^2, \qquad k = \frac{\omega}{c_p}$$

Because composites are often anisotropic, they produce phenomena not seen in heterogeneous isotropic materials such as steel or aluminum. In composites, the wave propagation velocity is not only dispersive, but also direction dependent. Also, structural elements such as stringers or cored sandwich panels can affect the attenuation properties of Lamb waves.

Lamb waves can be generated through a variety of means, including but not limited to ultrasonic probes, lasers, piezoelectric transducers, FBGs, and MFCs. In this research, PZTs were used for their nearly negligible mass and volume, simplicity of integration, wide frequency range, and low cost. PZT-generated Lamb waves contain multiple modes, and sophisticated signal processing is required to distinguish these distinct modes (see section 1.4).

A proper Lamb mode for damage detection should feature non-dispersive characteristics, low attenuation, and high sensitivity. It has been found in the literature that narrow bandwidth input signals are able to prevent dispersion and for this reason windowed tonebursts, as opposed to pulses, are ideal for the Lamb wave generation signal [16]. Often times, the S_0 and A_0 modes are used for damage detection. S_0 modes react with reasonable sensitivity to defects anywhere

in the thickness of a test specimen whereas A_0 is more suitable to the detection of surface damages such as matrix cracking and corrosion [16].

Unlike the S_0 and A_0 modes, mode conversion, a combination of S_0 and A_0 modes, occurs as a result of discontinuities in the material, such as sudden thickness changes or delaminations. These interactions are demonstrated in Figure 2 for mode conversion of the S_0 mode. When the S_0 mode encounters the thickness change of the stiffener (Figure 2a), new S_0 and A_0 modes are created, and the S_0 mode also reflects and scatters. In addition to the reflected S_0 modes, a new converted mode is created, which is a combination of S_0 and A_0 modes. Similarly, when the S_0 mode encounters a delamination (Figure 2b), the discontinuity creates converted modes. Although subtle differences in the S_0 and A_0 modes can be recorded and reviewed, the mode conversion (MC) offers a strong damage feature that would not have otherwise resulted if not for the presence of damage. When comparing data sets recorded from a test specimen in a healthy and damaged state, discovering the presence of a new converted mode is a strong indicator of damage.
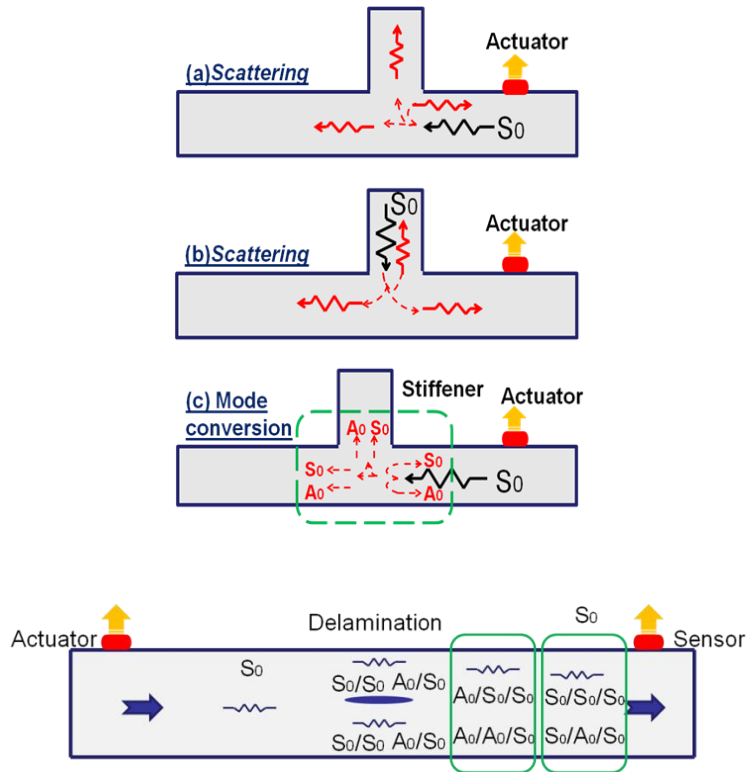
Figure 2. a) scattering and mode conversion due to stiffener interaction. b)

mode conversion due to delamination

1.1.2 Lamb wave detection research

The use of PZTs, which utilize guided waves to detect damage, has been investigated by many researchers [21-27]. Commonly used methods of determining the existence and location of damage are the correlation approach and time of flight (ToF) analysis.

The correlation approach directly compares data collected from the sensor array on the baseline test specimen with data from a specimen with damage. From this comparison, a damage index is defined, which is used not only as an indicator of damage, but also as a means of localizing the damage. When the data from

both healthy and damaged specimen come from the same test structure and the operating and environmental influences can be controlled, this becomes a useful detection technique. This technique is also very attractive for use in complex composite structures because the evaluation of the multifarious dispersion and attenuation characteristics of these structures are not needed. Lu [21] and Wang [22] used the correlation approach to detect and localize damage in stiffened composite panels based on a tomographical probability of damage algorithm developed by Zhao [28]. However, these methods introduced uncertainty under changing environmental conditions, as shown in the work by Michaels [23]. This work demonstrates that even small temperature fluctuations can mask the influence of damage on the data set when using statistical means of comparison such as correlation, covariance, or mean squared error as the damage index.

Time of flight (ToF), or time of arrival, methods are attractive because of how well they work with the underlying principles of Lamb wave sensing techniques. When a Lamb wave is produced, it results in at least two waveforms, the lowest order of which are the symmetric, S_0, and anti-symmetric, A_0, modes. When these two modes interact with boundaries, reflections occur, and when the modes interact with thickness changes, such as thickness change incurred due to a delamination, new modes result. These new modes are referred to as mode conversions (MC) and are comprised of combinations of S_0 and A_0 modes.

The reflected S_0 and A_0 modes as well as the MC can be used to determine the existence of damage by comparing the times at which these modes are received by the sensors in the benchmark data compared to their respective arrival

9

times in the damaged data set [29]. By noting the changes in the time of occurrence of the S_0 and A_0 modes and noting the appearance of any new reflections or converted modes, the presence of damage can be determined. Lu, et al. [24] successfully employed the ToF technique to detect cracks in aluminum plates by noting the times of the S_0 reflections as a result of a crack. Sohn, et al. [25], extracted the useful information necessary to provide proof that damage existed by looking at the influence of damage on the A_0 mode. Su and Ye [26] used the lowest order shear mode produced by damage to detect the presence of damage. A drawback of the ToF method is that in feature dense geometries, a large amount of post processing is necessary. However, this drawback can be reduced by performing an early wave propagation analysis and utilizing the knowledge of the test specimen geometry. If the MC or new reflected mode can be found in the time domain, ToF localization methods can be used to provide very accurate damage position estimates [15].

An important reason for developing damage detection techniques is to account for the variability that arises from different sources, such as operating conditions, sensing systems, material properties of the constituents, computation, and environmental influences [30-34]. Several methods exist that limit or normalize the effects of temperature [35-39]. Lu and Michaels [35] developed an adaptive baseline approach for damage detection over a range of temperatures. However, most of these methods require a large amount of data.

1.2   Damage Detection

Lamb wave-based damage detection is fundamentally based on the interpretation of the captured wave signals. For instance, in order to properly extract the key features necessary to determine the existence of damage, advanced signal processing techniques must be used. The chosen method must be able to account for noise, structural vibration, and overlapping of multiple modes. Currently, there are several methods of detection, based on correlation, time, frequency and integrated time-frequency.

1.2.1   Correlation analysis

Correlation analysis of data directly compares a damaged signal to a benchmark signal using any number of different indices to measure the change. Michaels and Michaels [39] were able to detect damage by subtracting these signals from one another and computing the peak magnitude or the energy of the residual signal. Gao et al [40] defined a damage index A where $A = 1 - \rho$ and ρ is the correlation coefficient between the two compared signals. This method is only dependent on signal shape changes. Michaels [23] created a damage index based on the normalized square error, the correlation coefficient, and the loss of local coherence, which is how far the average local coherence drops below unity. These methods are very effective if damage is the only contributing factor on the change of a signal. In most applications, however, this is rarely the case. In the work by Michaels [23], variations as a result of damage were found to be an order of

magnitude smaller than those caused by temperature variations, thereby requiring an advanced data normalization technique to adjust for this difference.

1.2.2   Direct time domain analysis

The direct time domain analysis of a signal can detect damage both globally and locally. Valdes and Soutis [41] located a delamination in a composite beam by measuring the change of ToF in the acquired Lamb signal. Sohn and Farrar [42] found that the difference in the signals in the time domain between a defective structure and benchmark structure was highest for sensor paths closest to the damage. Zang et al [43] captured the essential features from measured response signals by combining independent component analysis in the time domain and artificial neural networks (ANN). However, direct time-series analysis is normally incapable of appropriately isolating defect-scattered information from noise in different frequency bands.

1.2.3   Frequency analysis

The traditional Fourier transform (FT) or Fast Fourier transform (FFT) method provides 'global' information about the frequency content; it is suitable for signals with stationary frequency content, and has been used extensively for Lamb wave analysis [44-47]. However, since the frequency content of a Lamb wave signal varies in a time domain, this type of signal can be better represented in the time-frequency domain to extract time-varying frequency information. In

order to analyze the time-varying sensor response effectively, both time and frequency domain characteristics must be considered simultaneously. Thus, by combining the time and frequency domain data, Time-Frequency Representations (TFRs) characterize a given signal over the time-frequency plane, thereby yielding additional revealing information about the temporal localization of a signal's spectral components. Several TFR methods exist including, Short Time Fourier Transform (STFT), Wavelet Analysis, and Matching Pursuit Decomposition (MPD).

1.2.4 Time-frequency analysis

The STFT method was developed by Dennis Gabor to improve the efficiency of FT or FFT transforms for non-stationary signals [48]. This was accomplished by applying the basic FT to a small windowed section of the signal that was to be transformed. By continuously moving the short time interval along the time axis, STFT is able to map a time-dependent wave signal into a 2D representation. Although STFT provides temporal time-frequency resolution, a major issue is the resolution trade-off for the time and frequency domains [48].

Wavelet analysis uses a wavelet, a piece of waveform with limited duration whose average amplitude equals zero. It also maps a time-dependent signal into a 2D representation with scale and time, rather than a direct time-frequency view. However, the scale can be connected with frequency by determining the scale value at which a scalogram reaches its maximum [49]. Continuous wavelet transform (CWT) and discrete wavelet transform (DWT) are

two typical forms of WT., Lemistre and Balageas [50] and Su et al. [26] used WT to locate delamination in composite laminates. Kessler et al. [51] applied WT to a PZT-generated A_0 mode acquired from a sandwich beam for the detection of delamination. However, the fundamental principles of WT are not well adapted to represent functions whose FT have a narrow high frequency support. With WT, it is difficult to detect and identify signal patterns from just the expansion coefficients [52].

The Matching Pursuit Decomposition (MPD) is a time-frequency based technique that *decomposes* a signal into highly localized time-frequency atoms and can provide a highly concentrated TFR [52]. MPD is better suited than WT because it is a flexible decomposition that is able to represent a signal whose localizations in time and frequency vary widely. MPD is an iterative algorithm that decomposes any signal into a linear expansion of waveforms that belong to a redundant dictionary. The MPD dictionary consists of a collection of time-frequency atoms that are the dilated (time-scaled), translated (time-shifted), and modulated (frequency-shifted) versions of a single basic atom. The basic atom is often chosen to be a Gaussian signal because Gaussian signals are the most concentrated signals in both time and frequency. The MPD method has been applied to SHM for both metal and composite structures. Das et al. [29] developed a Monte Carlo MPD method for damage quantification in simple composite structures, but the developed algorithm was only validated by detecting and localizing damages in 12-inch long composite beams. Chakraborty et al. [53] used an MPD algorithm to classify the fastener failure damage in aluminum

plates. Liu et al. [15] used MPD to detect damage in stiffened composite panels with large delaminations and was able to localize the damage on a global scale. It is for these reasons that the MPD algorithm is used as the time-frequency analysis tool in this research to calculate the damage features in the data.

To decompose a signal using MPD, it must first be shown that for Lamb waves, the signal with finite energy, $s(t)$, can be decomposed into a linear combination of time-frequency atoms. This type of infinite approximations can be written as,

$$s(t) = \sum_{i=0}^{\infty} \beta_i\, g_i(t)$$

2)

where $g_i(t)$ is the time-frequency atom (sub-waveform) selected from the MPD dictionary D and β_i is the corresponding expansion coefficient. The finite linear combination of these time-frequency atoms can be used to provide an approximation of the signal with high accuracy. After N iterations, the resulting expansion can be expressed as,

$$s_N(t) = \sum_{i=0}^{N} \beta_i\, g_i(t)$$

3)

and the residual signal $Rs_N(t)$ with N iterations is,

$$Rs_N(t) = s(t) - s_N(t) = s(t) - \sum_{i=1}^{N} \beta_i\, g_i(t)$$

4)

Because the signal has finite energy, the energy of the approximated signal is also preserved. The energy conservation can be expressed as,

15

$$\|s(t)\|^2 = \sum_{i=0}^{N} \|s_N(t)\|^2 + \|Rs_N(t)\|^2 \qquad 5)$$

In order to find the best match between the signal and time-frequency atoms, the inner product of the signal and each time-frequency atom is calculated. Let $g(t) \in A$, where the signal, $s(t)$, can be decomposed into wavelets as shown by,

$$s(t) = \langle s(t), g(t) \rangle \, g(t) + Rs \qquad 6)$$

where Rs is the residual signal after approximation using the time-frequency atom, $g(t)$. To minimize the energy of Rs, the proper $g(t)$ is defined to satisfy the equation,

$$|\langle s(t), g(t) \rangle| \geq \beta \sup|\langle s(t), g(t) \rangle| \qquad 7)$$

where β is an optimality factor that satisfies $0 < \beta \leq 1$, $\sup|\langle s(t), g(t) \rangle|$ is the least upper bound of the inner product of $\langle s(t), g(t) \rangle$. The decomposition of signal $s(t)$ is completed by successive calculation with time-frequency atoms from the dictionary. Let $g_i(t)$ be the time-frequency atom of the ith iteration, and the approximated signal at this iteration is,

$$s_i(t) = \langle Rs_i(t), g_i(t) \rangle \qquad 8)$$

When i=0, let $Rs_0 = e(t)$. According to Equations 3, 6 and 8, the approximated signal with a total of N iterations is,

$$s_N(t) = \sum_{i=1}^{N} \langle Rs_i(t), g_i(t) \rangle \qquad 9)$$

and the original signal can be expressed as,

16

$$s(t) = \sum_{i=1}^{N} \langle Rs_i(t), g_i(t) \rangle + Rs_N \qquad \text{10)}$$

where Rs_N is the residual signal at the Nth iteration. Although a redundant dictionary can provide flexible decomposition of the signal, the computational cost is consequentially high. To reduce the number of unnecessary time-frequency atoms, a modified MPD algorithm is used. The time-frequency dictionary of the MPD algorithm is optimized based on the features of the Lamb wave signals from the structures being interrogated. Limited sub-waveforms that best represent the original signal are included in the dictionary. By using the optimized atom dictionary, the original signal can still be efficiently decomposed with high local time-frequency resolution.

The actuation signal used in the experiments conducted here is a cosine burst wave. According to the Lamb wave theory, only S_0, A_0 and the related converted modes exist as sub-waveforms. These sub-waveforms can be expressed as,

$$g(t) = e^{-\beta(t-\tau)^2} \cos(2\pi ft) \qquad \text{11)}$$

where the constant β defines the width of the burst wave and f is the central frequency. S_0, A_0, reflected S_0 and A_0 waves, and the related converted modes can be obtained by the dilation and translation of the basic sub-waveform [29, 52]. This procedure reduces the size of the MPD dictionary significantly. It must be noted that the MPD algorithm efficiently yields a compact representation of the burst wave signals in terms of selected basic atoms in the dictionary. Therefore, it

17

reduces the computational cost significantly. In addition, the noise is filtered out because the noise waveforms are typically orthogonal to the selected atoms. Using the refined MPD algorithm, the guided wave signals from different sensors can be represented in the same time-frequency domain. The difference of ToFs between sensors can be compared and accurately calculated. This ToF information is used as input information for the damage location optimization code's objective equations.

1.3   Damage Localization

Damage localization methods used for analyzing the features extracted from the previously listed detection methods can either be forward or inverse. Forward analysis is a logically conducted method with unique solutions where the results from inverse analysis are often ambiguous and difficult to solve rationally [16]. ToF localization methods are a forward method and are based on the time lag between the sensor catching the incident signal and the damage reflection and are based on simple triangulation (Eq. 12).

$$\frac{\sqrt{(x-x_i)^2 + (y-y_i)^2}}{V_{S_i}} + \frac{\sqrt{x^2 + y^2}}{V_{S_0}} - \frac{\sqrt{x_i^2 + y_i^2}}{V_{S_0}} = T_{1-i} \qquad 12)$$

where (x,y) are the coordinates of the damage, (x_i, y_i) are the coordinates of the ith transducer, V_{Si} is the velocity of the damage reflected signal, V_{S0} is the velocity of the S_0 mode, and T_{1-i} is the time lag for sensor path P_1-P_i. Y Lu et al [24] used this

technique to localize cracks in aluminum plates. Baseline free methods that use time reversal [54-55] to determine the time lag between a healthy output signal and the returned damaged signal have also been studied. These methods are very accurate if the wave velocities are well understood, but they become more difficult to use in anisotropic materials and even more difficult when the material is feature dense.

In the case of complex samples, tomography methods (in inverse analysis) work very well because there is no need for the time information, and thus wave velocities. The tomography technique developed by Zhao [28], the reconstruction algorithm for probabilistic inspection of defects (RAPID), first determines the correlation coefficients between a healthy set of sensor path data and a damaged set of data. In this method, the correlation coefficients are determined for each sensor path and a damage index is developed based on that information. Then a probabilistic tomography approach is used. The structure is discretized, and the probability of damage at each grid point is calculated. The relative distance between each grid point and sensor path is calculated. The influence of the sensor path on the grid point of interest is then weighted depending on the relative distance because each sensor path creates an elliptical interrogation area, and grid points that fall out of this area are not of interest. The weighted value for each sensor path is then multiplied by its associated damage index. The resulting product is calculated for each sensor path relative to one grid point and then summed for all the sensor paths, leading to the probability of damage at each grid

point. This process is repeated until damage probabilities have been calculated for every point of interest on the panel. Equation 13 describes this

$$P(x,y) = \sum_{k=1}^{n} \left[A_k \cdot \left(W\left(R_k(x,y)\right)\right)\right] \qquad 13)$$

where $P(x,y)$ is the probability of damage at each grid point, A_k is the damage index for each sensor path, k, n is the number of sensor paths, and $W(R_k(x,y))$ is the weighted relative distance.

The weighted relative distance is controlled by a scalar, β, which controls the size of the elliptical interrogation area surrounding each sensor path. A large value for β will allow many sensor paths to contribute to $P(x,y)$, while a small value for β will not include enough. Because of this, it is necessary to determine a reasonable value for β. The relative distance, $R_k(x,y)$, and the weighted value, $W(R_k(x,y))$, are defined as

$$R(x,y) = \frac{D_{ak} + D_{sk}}{D_k} - 1 \qquad 14)$$

$$W(R(x,y)) = \left| \begin{array}{l} \left(1 - \dfrac{R(x,y)}{\beta}\right) \ \text{if} \ R(x,y) < \beta \\[2ex] 0 \ \text{if} \ R(x,y) \geq \beta \end{array} \right. \qquad 15)$$

where D_{ak} is the distance between the grid point and the actuator, D_{sk} is the distance between the grid point and the sensor, and D_k is the length of the sensor

path. Thus, a grid point that lies directly on the line connecting a sensor path will yield a value of $W(R_k(x,y)) = 1$, and a grid point lying outside the ellipse created by the sensor path will yield a value of zero. This is because a sensor path that crosses a grid point should have the most influence on $P(x,y)$ for that grid point, and a sensor path far away from that grid point should have no influence [28].

1.4   Objectives

The goal of this research is to investigate the use of mode conversions as a damage feature for determining the existence and location of damage in a blade stiffened anisotropic composite panel. The first experiment uses the tomography approach with the mode conversion energy as the damage index. A single anisotropic stiffened panel is used to highlight the ability of the damage index to not succumb to the complexity of the response signal from a feature dense sample while limiting some experimental variability. The second experiment addresses the effect of temperature in damage detection while also introducing the manufacturing variability by collecting data from two different samples (healthy and with delamination). This is different from other approaches where the effect of variability is limited by using the same sample. It is posited that by extracting only the times of the mode conversions and new reflections as a result of damage, the existence of damage can be inferred regardless of temperature change.

CHAPTER 2

DAMAGE INDEXING AND LOCALIZATION IN A STIFFENED PANEL

FROM MODE CONVERSION

In structural health monitoring of aerospace components, such as stiffened panels, detection and localization of damage is an important issue. This chapter presents a methodology for determining the existence and location of low velocity impact damage in a stiffened composite panel. Using a matching pursuit decomposition algorithm, converted modes due to damage were extracted in the time-frequency domain. The energy of the converted mode was then used in conjunction with a probabilistic tomography approach that was able to localize the damage with a high level of accuracy. The main goal of this research was to determine if mode conversion energy can be used as a strong damage index in order to use a computationally efficient tomography localization approach. Section 2.1 provides the experimental setup, Section 2.2 shows the results of the study and offers some discussion about the findings, and Section 2.3 provides some concluding remarks about this experiment.

2.1   Experimental Setup

2.1.1   Panel fabrication

A stiffened carbon fiber reinforced plastic (CFRP) panel was made in house out of FiberGlast 3K plain weave fabric. A two-part epoxy, FS-A23 (resin) and FS-B412 (hardener) from Epoxy System Inc. was used as the matrix with a

3:1 mixture ratio of resin to hardener. The panel was co-cured with two three ply $[0]_3$ sections (Figure 3) to create an anisotropic $[0]_6$ laminate. This was done by first laying up three plies on a baseplate, and then laying three plies on three separate tools and placing them together while clamping the sides across the stiffeners to even the stiffener thickness. The plates were cured in a heated press for eight hours at a temperature of 38°C under a pressure of 1470 kPa. The panels were fabricated with a plate and stiffener thickness of 1.30 ± 0.10mm. After the cure cycle, the panel was removed and cut to dimensions of 314.33 mm along the stiffener length, and 306.10 mm in the transverse direction with the stiffeners spaced an equal 50.80 mm from the edge (Figure 4). Damage was introduced to the panel after data was collected for a benchmark data set in the form of low velocity impacts along the stiffener (Figure 4)
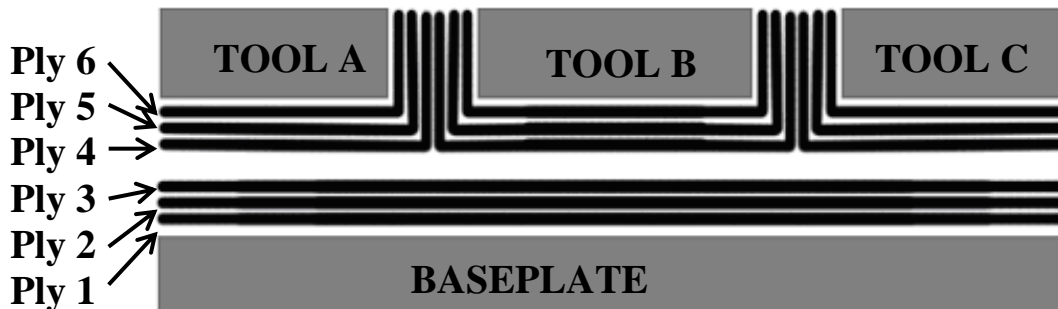

Figure 3. Panel layup sequence
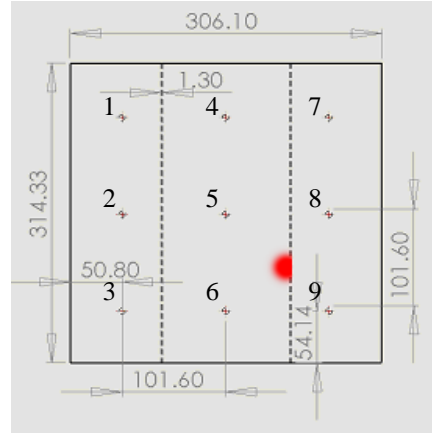
Figure 4. Panel dimensions (mm) and location of damage marked in red

2.1.2   Interrogation system

Nine PZT wafers were adhered to the surface of the panel in an evenly distributed grid on the stiffened side. The PZTs were centered and spaced 101.6 mm from one another along and across the stiffener direction (Figure 4). The panel was then interrogated using an NI 5412 waveform generator to create the excitation signal. The sensor signals were captured using a NI 5105 digitizer at a sampling frequency of 20 MHz. In order to optimize the central frequency of the actuation signal, several actuation signals were generated using central frequencies varying from 10 to 300 kHz in 10 kHz increments. Five observations were recorded at each frequency and then averaged to reduce the sampling error. After an initial review of the data, a central frequency of 180 kHz was used for actuation for the main testing. This frequency was chosen because of the high mode separation found at this frequency after a time-domain analyses of the data found at each tested frequency.

2.1.3   Test procedure

A round robin approach was used, and each PZT on the panel was used in turn as the actuator and sensor. This resulted in a total of 44 sensor paths (Figure 5). Maximizing the number of sensor paths increases the probability of detecting damage, but this number needs to be well thought-out because of the computational cost related to the number of sensors. After recording the healthy baseline data, the healthy panel was then subjected to low velocity impact damage to simulate a tool drop. Flash thermography was used to record and visualize the damage (Figure 6). The same method used to record the healthy baseline data was again used to record data from the damaged sample.
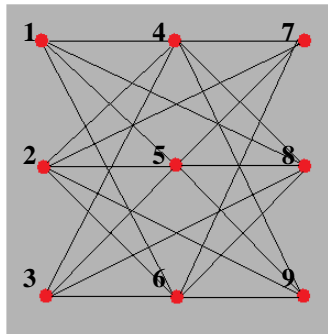
Figure 5. Panel sensor paths (paths denote both a sending and receiving path)
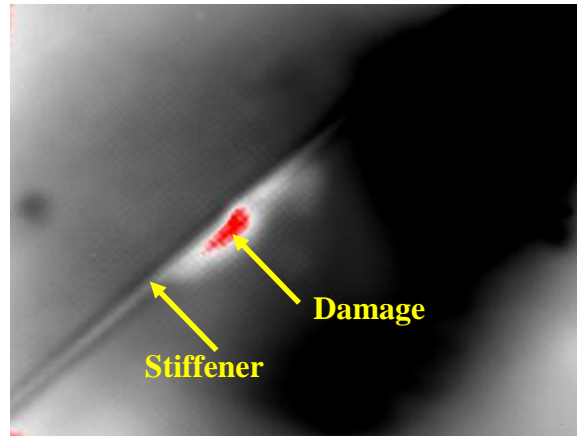
Figure 6. Flash Thermography imaging of induced damage

2.2 Results and Discussion

2.2.1 Time-frequency response of recording

The MPD algorithm was used to obtain the TFR plots for both healthy and damage states. This was done by adjusting the shift and scale parameters in the MPD code (Appendix A) to create a dictionary that best decomposed the signal while enhancing computational efficiency. It was found that values for "amin" and "amax" (controlling the width in the time domain of the atom) were best set at 1.5 and 3, respectively, and "fmax" and "fmin" (controlling the width of the atom in the frequency domain) were best set at 160kHz and 200 kHz, respectively. As seen in Figure 7 only 10 iterations were necessary to decompose ~95% of the energy.
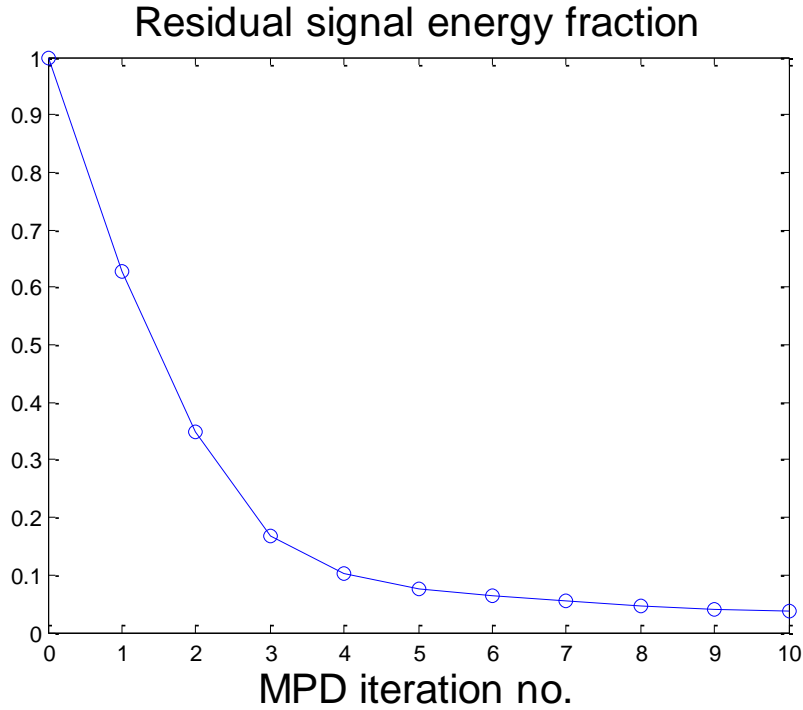
Figure 7. Residual Energy for MPD on path 5-8

Figure 8 shows a TFR from the healthy and damaged data from path 1-8 and Figure 9 shows a TFR from the healthy and damaged data from path 5-8. Path 1-8 is not near the damage, whereas path 5-8 almost crosses the damage location. Comparing the similarity of the TFRs (a) and (b) in Figures 8 and 9, it is evident that damage exists along or near the path of 5-8 and no damage exists near path 1-8. Of the 44 recorded paths, only 22 were investigated after this point due to symmetry (path 1-8 is identical to path 8-1).
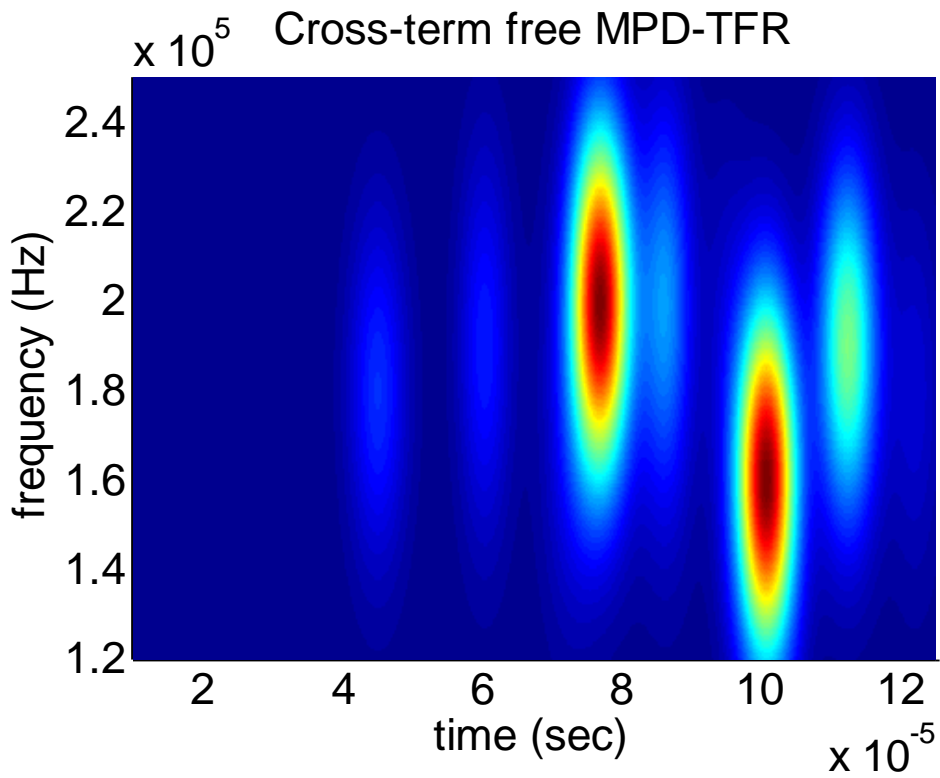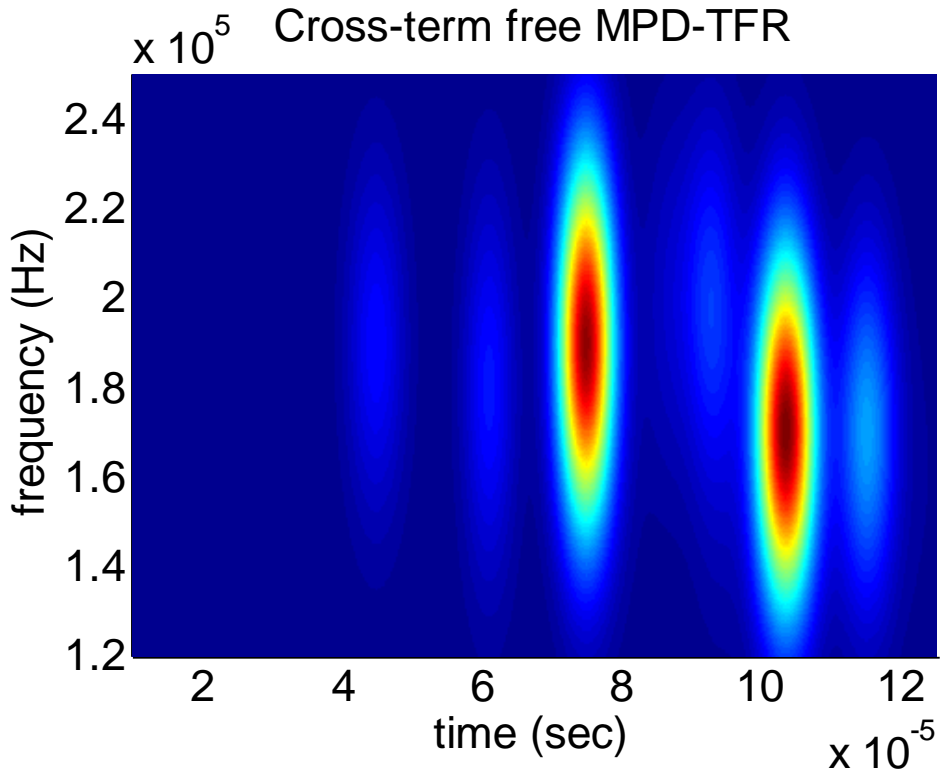
Figure 8. (a) Healthy panel TFR path 1-8 (b) damaged panel TFR path 1-8
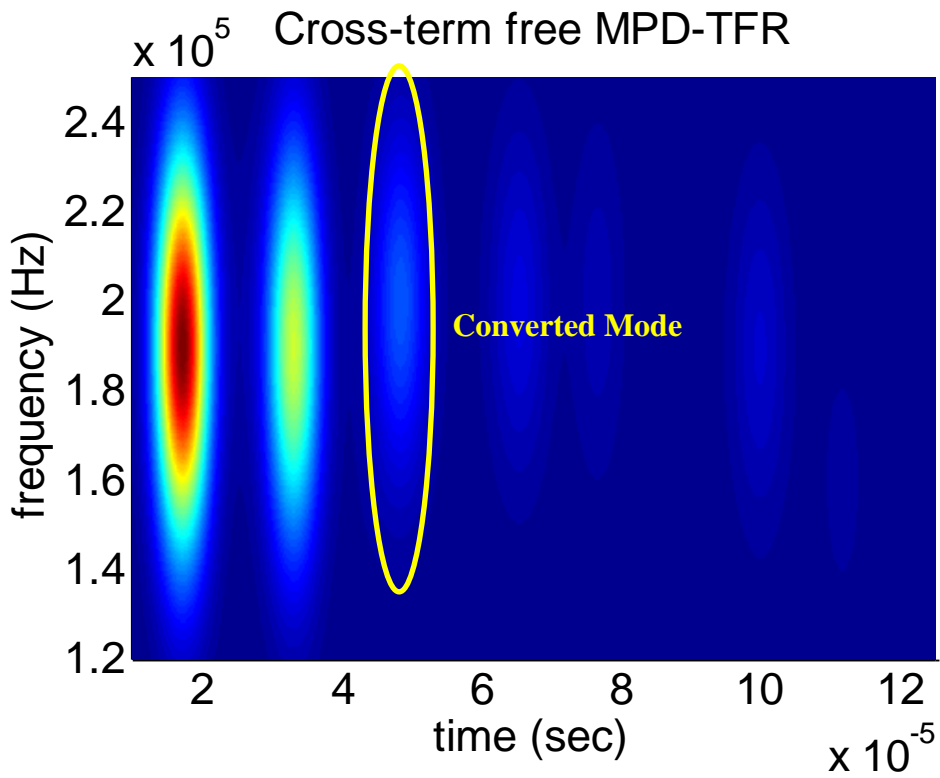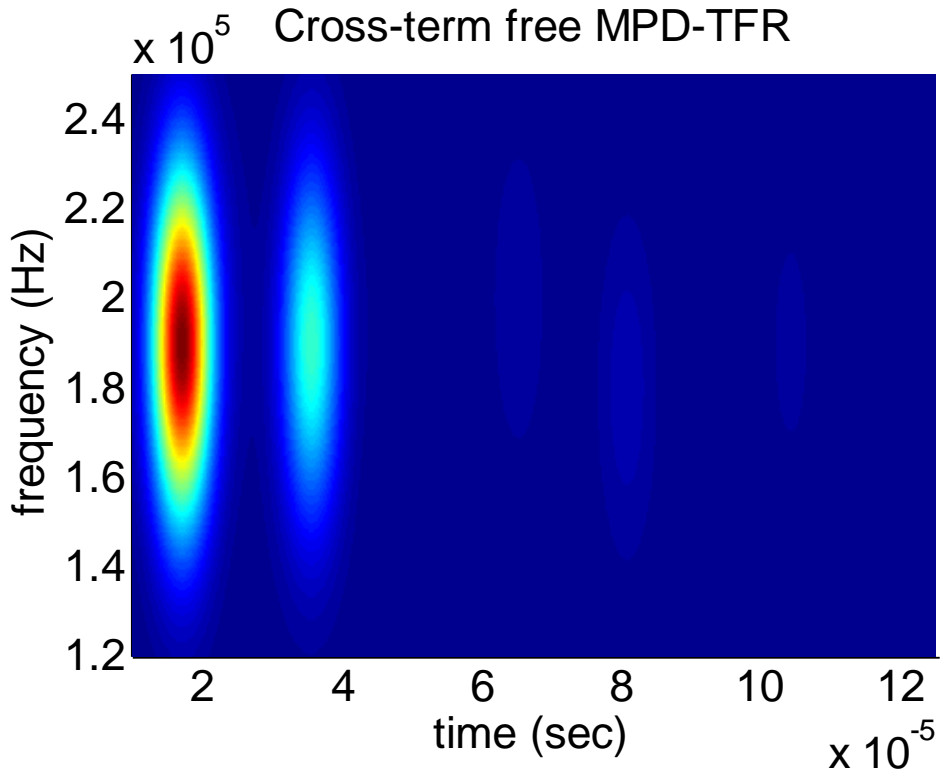
Figure 9. (a) Healthy panel TFR path 5-8 (b) damaged panel TFR path 5-8

2.2.2 Determination of damage index

From these TFR plots, damage indices were defined based upon the presence and strength of signal from the converted mode. The TFR data is then normalized in the energy domain and the maximum normalized energy in the time domain from each TFR plot is compared. This was done by superimposing the energy curves from the healthy panel with that from the damaged panel (Appendix B). From this comparison, the energy difference can be calculated at the time of mode conversion (Figure 10) and the damage index can be defined. The maximum normalized energy from the mode conversion was used as the damage index because other damage indices listed in the introduction can be easily influenced by environmental changes and variability. From the research presented in Section 1.2, it has been shown that mode conversion offers a strong indicator of damage and is least affected by influences other than damage.
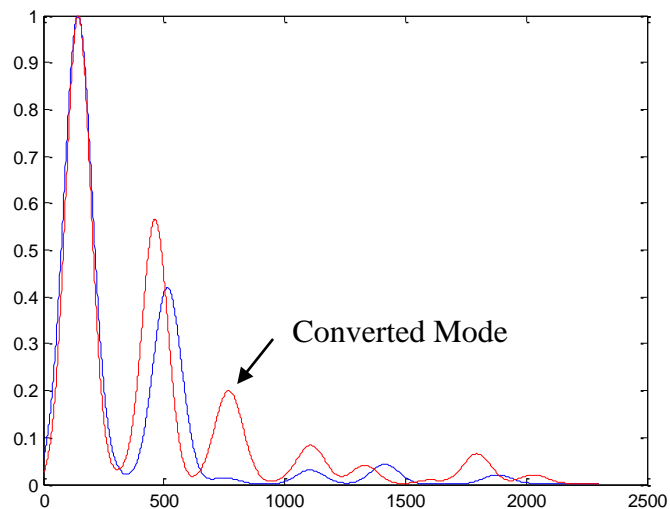
Figure 10. Maximum normalized energy over sample size for path 5-8

30

The damage indices for damaged sensor paths are shown in Figure 11. The other sensor paths not shown in Figure 11 have negligible or no converted mode signatures. Figure 11 illustrates that sensor paths that cross directly through the damage have a much higher damage index than the sensor paths that travel farther from the damage. For example, sensor path 5-9 passes directly through the damage and has the highest damage index, whereas sensor path 6-9 passes close to but below the damage and it has a much smaller damage index. Therefore the localization will predict a damage location closer to sensor path 5-9 than sensor path 6-9.
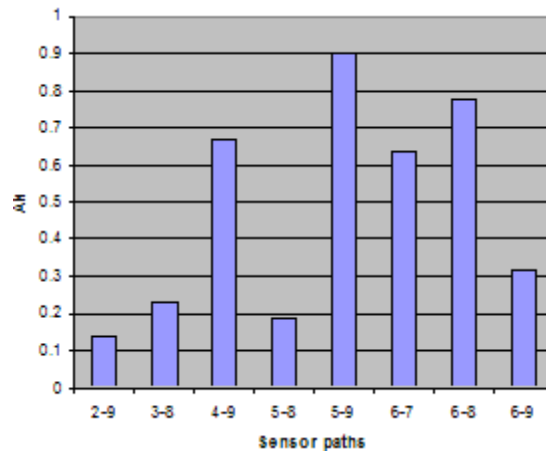
Figure 11. Damage indices, A_k, for damaged paths based upon MC energy

While some of the previous works [21, 22, 28] are based on the influence of every sensor path, this method uses only the sensor paths that display a converted mode due to damage. This, in a sense, places a threshold on the data

and leads to more accurate results since the influence from negligible sensor paths can otherwise skew the results.

2.2.3   Tomographic localization

The novelty of the procedure developed in this research is the use of the converted mode to determine the damage index, A_k, where k is the number of sensor paths displaying mode conversion. This is because correlation coefficients that are based on the comparison of two raw signals do not always yield reliable results. Influences such as noise and environmental changes can have a large effect in hiding the presence of damage or cause a large enough change in the signals that zero correlation between the healthy state and damaged state may result [27]. To overcome this issue, MPD is used to determine the true response signal changes between the healthy and damaged state. When the TFR plots between baseline and damaged data are compared, the mode conversion as a result of damage can be identified. The energy in the converted mode can then be used to quantify the influence of damage on each specific sensor path. From this, a value for A_k can be defined, and P(x,y) can be determined similar to the RAPID algorithm developed by Zhao [28] (Appendix C).

2.2.4   Localization results

As previously mentioned, a proper value of β must be determined to include enough damaged sensor paths to accurately predict the damage location.

32

Previous work by Wang [22] demonstrated that a value of 1.05 was useful for sensor arrays similar in size to the one used in this experiment. However, a parametric study was conducted on the value of β to see how it affects the error distance of the results (Figure 12).
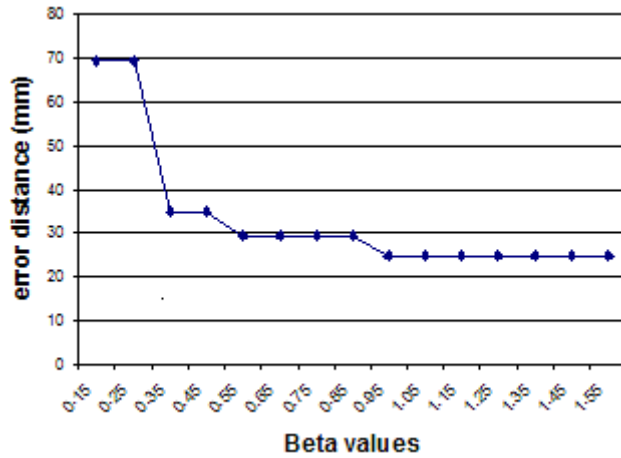
Figure 12. Effect of β on distance between the actual and predicted damage.

When β is small (0.15) then the interrogation area surrounding each sensor path is too small and not enough sensor paths are used to determine the probability of damage over the panel (Equation 15). This results in the damage being predicted at the sensor locations that carry the most damaged sensor paths (Sensors 6 and 9 for this experiment). Figure 13 illustrates the probability of damage distribution using $\beta = 0.15$. The true damage location is marked with a large blue cross and the predicted location is marked with a red cross. Although the predicted damage location is not very accurate, it is interesting to note that even with a poor choice for the value of β that the algorithm was still able to identify with certainty the correct quadrant that contains the damage.

33
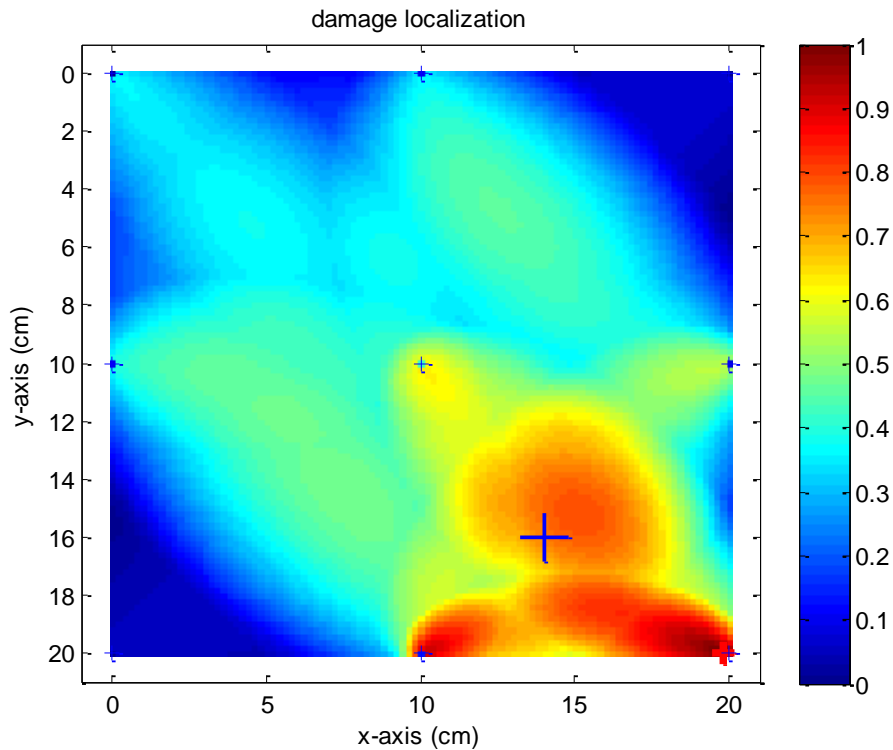
Figure 13. Localization results (β = 0.15)

As β is increased, the error value converges to 25 mm. Increasing β beyond 1.05 is not necessary because β = 1.05 includes the influence from all the sensor paths. If the panel were larger, larger values of β would likely not be needed because sensor paths further out from the damage would not display a converted mode. The result from the localization technique using β = 1.05 is presented in Figure 14. The center of damage is marked with a blue cross and a red cross marks the predicted damage point. Although the results were satisfactory (error <25 mm), additional sensor paths would increase this accuracy.
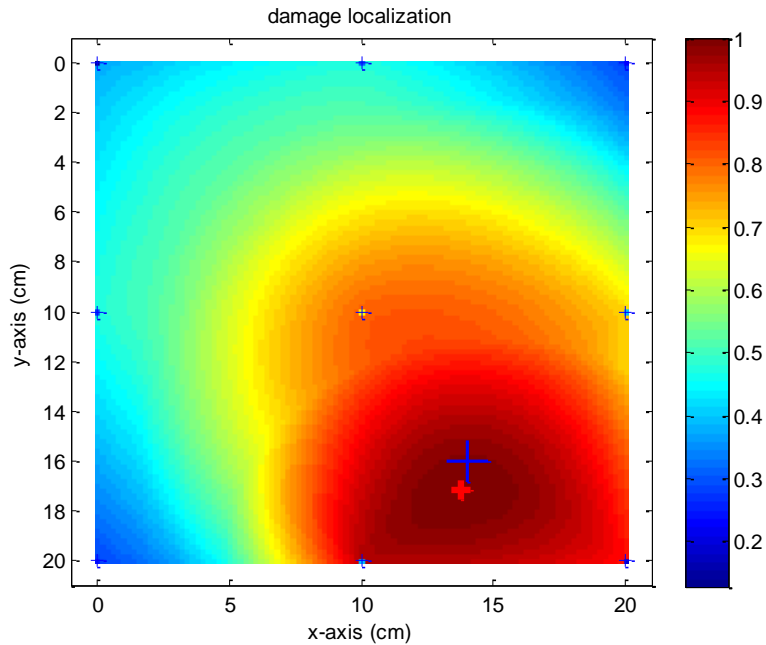
Figure 14. Localization results (β = 1.05)

It should also be noted that while introducing damage to the specimen, two of the PZTs were damaged and had to be replaced mid experiment (sensors 4 and 5). In localization methods that are baseline sensitive, this would have had a detrimental effect and new baseline data would have been necessary. This would be impossible after the introduction of damage. The robustness of this system exists because MPD is able to remove effects caused by slight differences in sensor characteristics and mode conversions will still exist regardless of small changes in response signal as a result of a new PZT.

2.4   Concluding Remarks

In this experiment, low velocity impact damage in a CFRP stiffened panel was detected and localized using Lamb wave based tomography. A nine node sensor network was used to collect data from the stiffened panel. An MPD algorithm was then used to generate TFR plots for a baseline and damaged data set so that the presence of converted Lamb wave modes could be identified. A damage index was calculated for sensor paths that showed the presence of a converted mode. The damage indices, based on the energy of the converted modes, were used in conjunction with a probabilistic tomography algorithm to localize the damage. Using only nine sensors, this method was able to accurately locate the damage within 25 mm on a stiffened panel. The novelty of this approach is its ability to accurately predict the location of damage in a complex structure without the need for calculating wave velocity.

CHAPTER 3

LAMB WAVE BASED FEATURE EXTRACTION OF DAMAGE IN A

STIFFENED COMPOSITE PANEL UNDER VARYING TEMPERATURE

This chapter presents a methodology for determining the existence of delaminations in complex composite structures. The changes in damage features due to changing temperature are investigated. A Lamb wave based active damage detection technique is used. The Matching Pursuit Decomposition (MPD), a time frequency based signal processing technique, is used for feature extraction. The signals from two different test structures, a healthy specimen and a specimen with seeded delamination, are compared to incorporate the effect of manufacturing variability. Tests are conducted under varying ambient temperature. The results obtained validate that modes shift linearly with the expansion of the samples and that mode conversions can be tracked and used for detecting delamination.

3.1   Experimental Setup

3.1.1   Laminate fabrication

Similar to the sample in Chapter 2, two stiffened carbon fiber reinforced plastic (CFRP) panels (306.1x314.33x1.3mm) were made out of $[0]_6$ plain weave and co-cured in three ply sections. A two-part epoxy, FS-A23 (resin) and FS-B412 (hardener) from Epoxy System Inc. was used as the matrix. The dimensions of the test structure and PZT locations are shown in Figure 1. The first panel, Panel A, represents the healthy sample. The second panel, Panel B, was created with a seeded delamination made of Teflon tape (7.5 mm x 7.5 mm) between plies

3 and 4 to simulate impact damage. Both panels were placed under heated press for 6 hours at 38°C and 1400 kPa. The location of the delamination was between the two stiffeners and roughly between PZT A and C. Figure 16 shows a flash thermography scan of the seeded delamination.
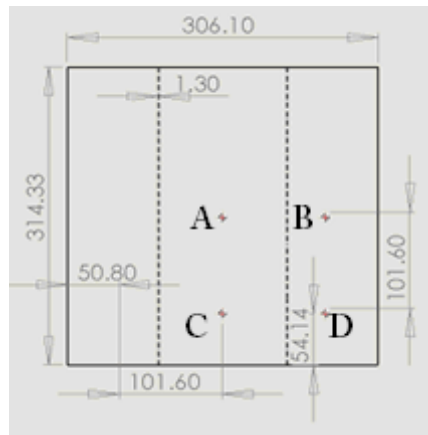
Figure 15. Panel dimensions and PZT locations (in mm)
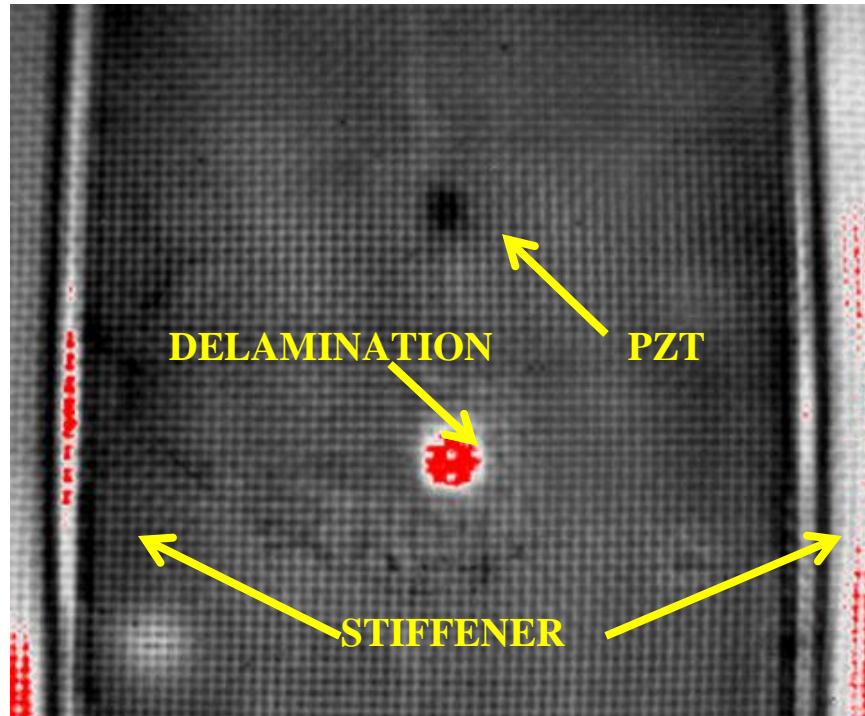
Figure 16. Flash thermography of delamination

3.1.2 Interrogation system

Nine piezoelectric transducers were evenly placed 101.6 mm apart on the panel (for tests not covered in this research), but only four were used for this testing (Figure 15). For all tests, each panel was interrogated using an NI 5412 waveform generator to create the excitation signal. The sensor signals were captured using an NI 5105 digitizer at a sampling frequency of 20 MHz. Five observations were recorded at each frequency and then averaged to reduce noise.

3.1.3 Testing methodology

A preliminary test was done on both panels to characterize the wave propagation in each panel at room temperature. PZT A was used as the actuator in both tests and the remaining PZTs were used as sensors. A Gaussian burst wave was used as the excitation signal ranging from 50-500 kHz in 25 kHz intervals so that dispersion curves could be constructed from data collected from PZT C. This was done to acquire the proper central frequency to use in future tests. The panels were supported by small cubes of rubber placed under each corner to offer a pseudo free-free boundary support. It can be seen in Figure 17 that although the damaged reflection can be found at a range of central frequencies, 425 kHz offers the least amount of dispersion between the fundamental modes. The differences in propagation velocities between the two panels, shown in Figure 17, are likely a result of subtle differences in boundaries, sensor placement, and material properties. Most noted was the difference in propagation velocity of the reflected S_0 modes, but this is a result of the existence of damage on the sensing path as

well as a small difference in the distance between PZT C and the edge of the panel between Panel A and B.

For the main test, Panels A and B were both placed in a Cascade TEK oven with the waveform generator source cable split to each panel and attached to PZT A. Data was recorded from PZTs B, C, and D simultaneously on both panels 0°, 45°, and 90°. Based on the findings of the preliminary test, 400, 425, and 450 kHz were chosen as the central frequencies and data was recorded at temperatures ranging from 20^oC to 80^oC in 10^oC intervals. Higher temperatures would cause failure in the PZT adhesive. Three central frequencies (400, 425, and 450 kHz) were used validate the hypothesis that dispersion properties will change under varying temperature.
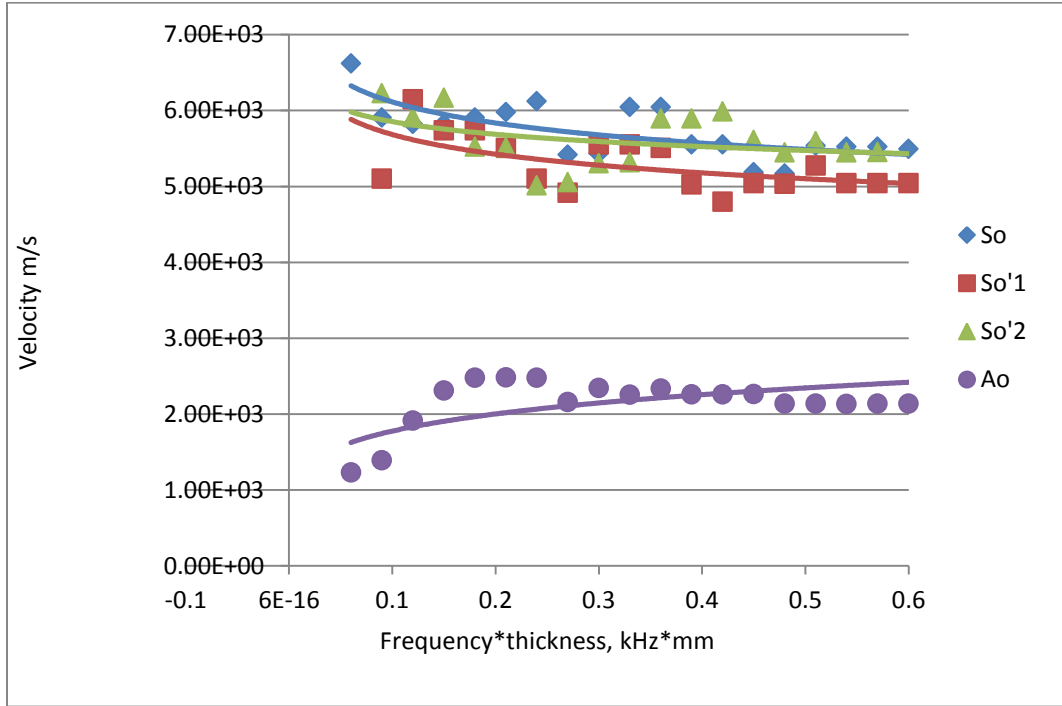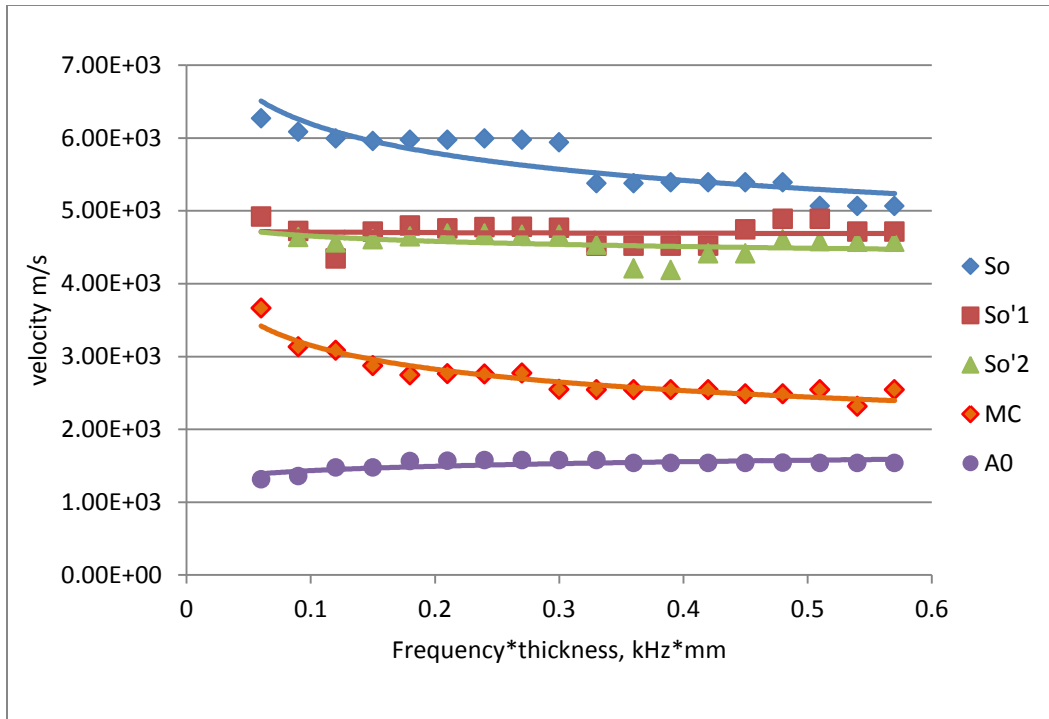
Figure 17. Dispersion curve for healthy (Panel A, left) and damaged (Panel

B, right) between PZT A and C

3.2 Results and Discussion

3.2.1 Initial wave propagation analysis results

Figure 18 shows the recorded data in its raw time domain form as collected from PZT C. It can be seen that the data is very different between the two panels even though they were manufactured to the same specifications. This is a result of variance in the form of sensor placement, boundary conditions, and slight differences in fabrication. Variability from sensor placement is not just a result of small differences in distance between the sensors, but also results if the

sensors are placed along different. Small differences in boundary conditions will also affect the ToF of mode reflections. Variations in material properties resulting from differences in fabrication (material thickness, volume fraction, ply orientation, etc.) will also affect the dispersive characteristics of the waves. By using MPD, these different signals can be decomposed to reveal their fundamental modes and reflections as well as their times of arrival.
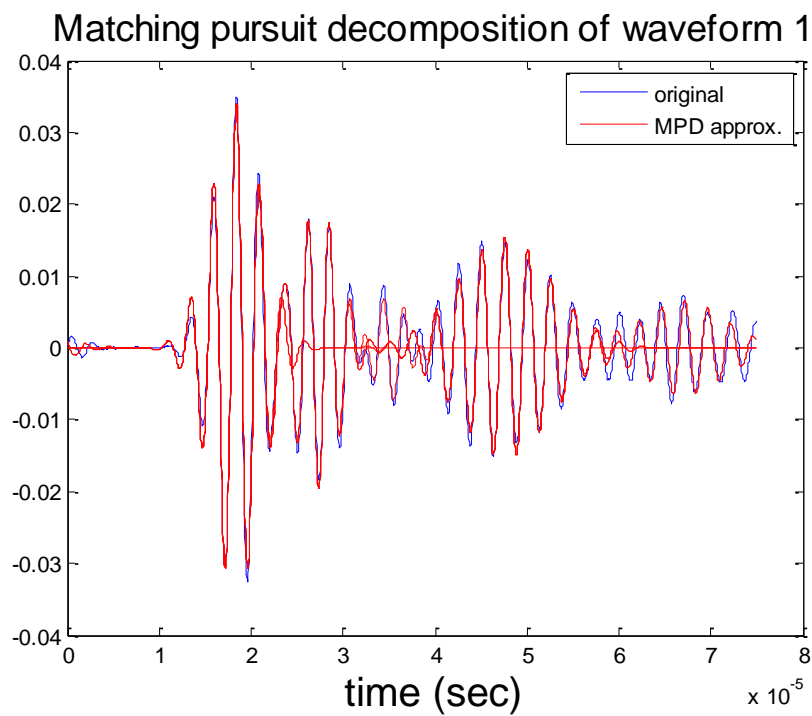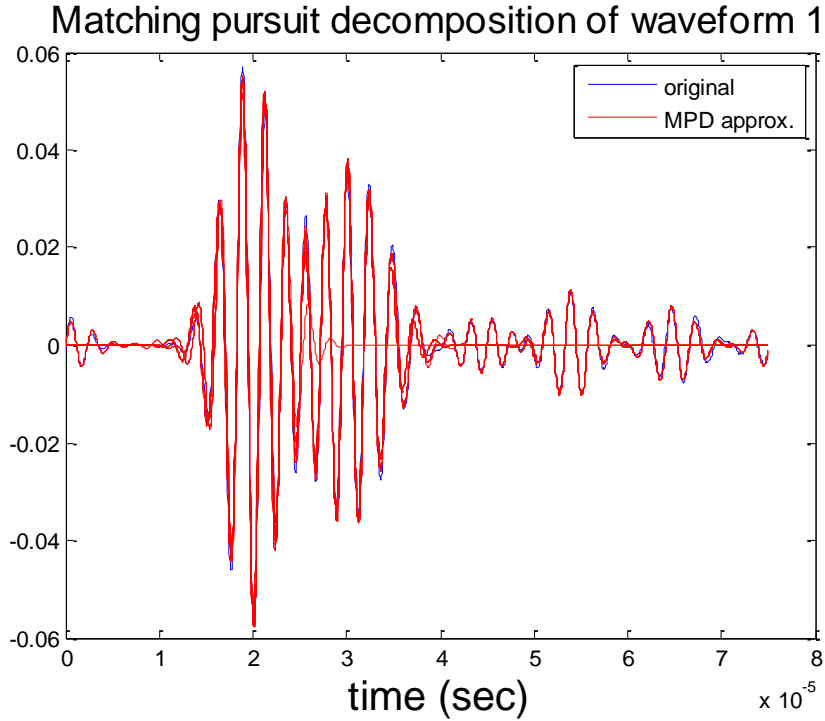
Figure 18. Time domain representation of Panel A (left) and Panel B (right)

between PZTs A and C

To effectively decompose the signal, the dictionary of time shift and frequency parameters that describe the elementary functions (or the atoms) had to be customized for each data set. The number of decomposition iterations necessary to capture the critical amount signal energy varied for each sensor path. Over-decomposing the signal can result in quantifying and characterizing the energy due to noise, which is undesired. A residual energy level of approximately 5% was used because it effectively reconstructed the sensor signals without noise. The residual energy as a function of decomposition iterations for two different panels is shown in Figure 19. The results of the MPD algorithm provide the central time for each atom (consequently Lamb wave mode) taken to be the mode

time of arrival. Once each atom has been decomposed, a time frequency representation (TFR) can be visualized in order to graphically understand the signal decomposition. Figure 20 shows the TFR of Panel A and B at 20°C for data collected from PZT C. As in Figure 18, the plots shown in Figure 20 bear only slight resemblance to each other. Simply overlaying these results for use in a cross-correlation technique would not yield representative result due to the variance. Using the time of arrival of the converted mode, damage identification can be accurately implemented.

Residual signal energy fraction

Residual signal energy fraction
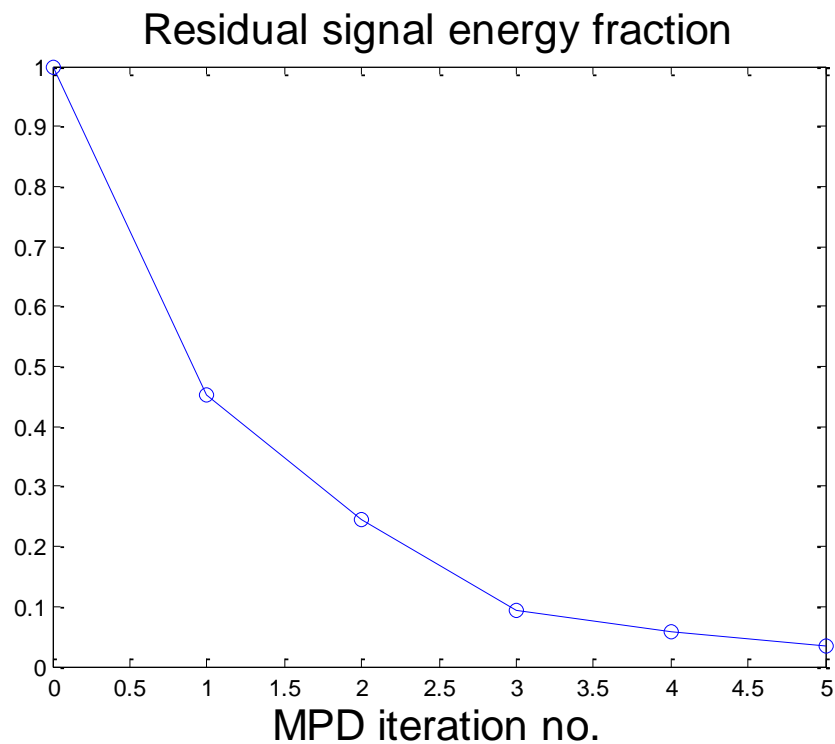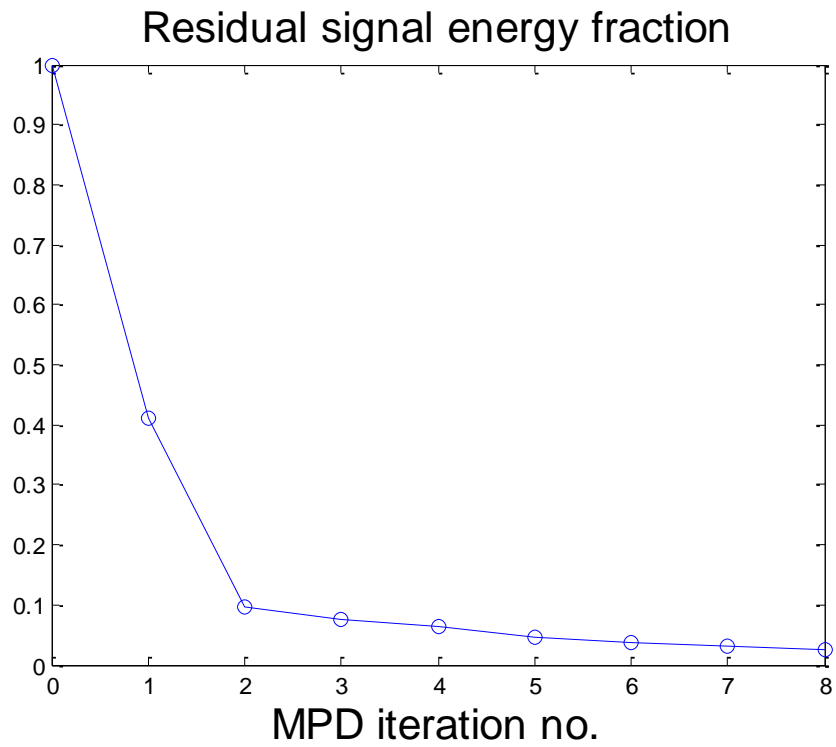
Figure 19. Residual Energy after N iterations for Panel A (left) and Panel B (right)

Cross-term free MPD-TFR
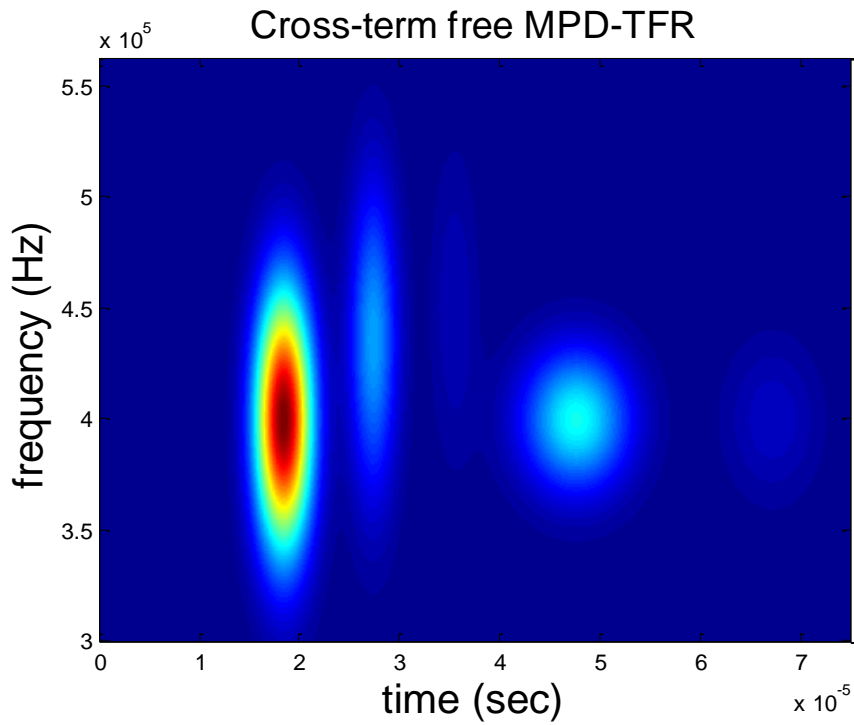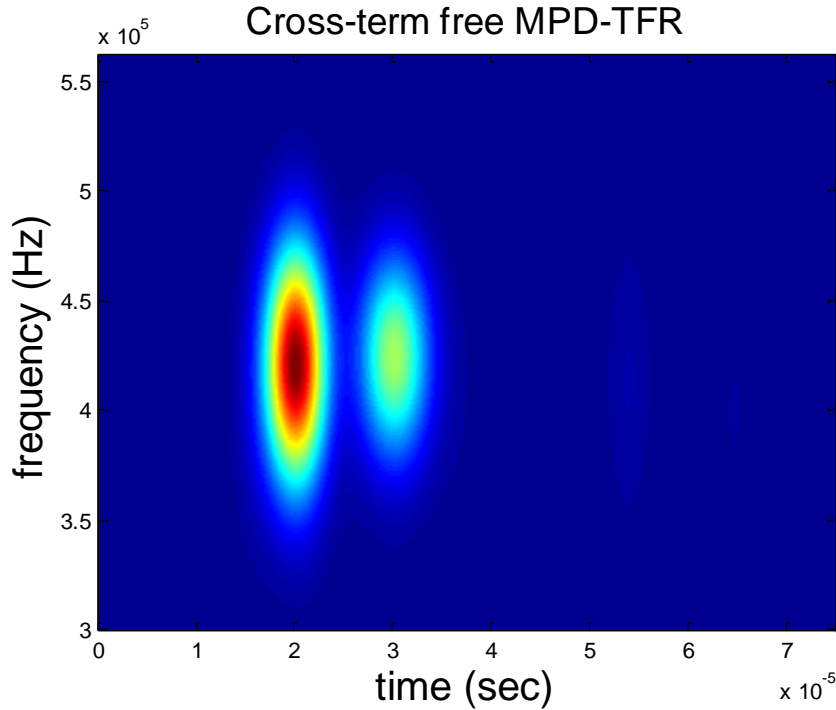
Figure 20. Time-frequency representation of data collected from PZT B for

Panel A (left) and Panel B (right)

3.2.2 Effects of temperature on recorded data

The time of flights of specific modes for the data collected from Panel A and

B is found by first observing the results of the preliminary test. The preliminary

test found the arrival times for the modes from Panel A and Panel B at 20°C. By

starting with the arrival times found in the preliminary test, wave propagation

analyses were performed on the data collected from the main test in a systematic

order from 20°C temperature to 80°C. This was done under the assumption that

although the arrival times would change, they would shift incrementally and

would be easier to track by starting with the room temperature data and moving

towards the higher temperature data sets. Figure 21 shows the difference in the

47

data collected from PZT C at 30$^\text{o}$C and 70$^\text{o}$C. Although the first mode, S$_0$, barely

changes, the other modes overlap, disappear, or weaken in signal strength due to

attenuation and dispersion effects caused by thermal expansion of the material.

However, the MPD code was able to reveal the location in time of the

fundamental modes for each panel and the converted modes for Panel B for every

temperature tested. The times of arrival for the modes in the data sets collected

from Panels A and B at PZT C are presented in Table 1, where the x in S'$_0$x

denotes the reflection number. The same was done for the data collected from

PZT B and D, but is not presented in this paper because the trends in the results

were markedly similar.

48
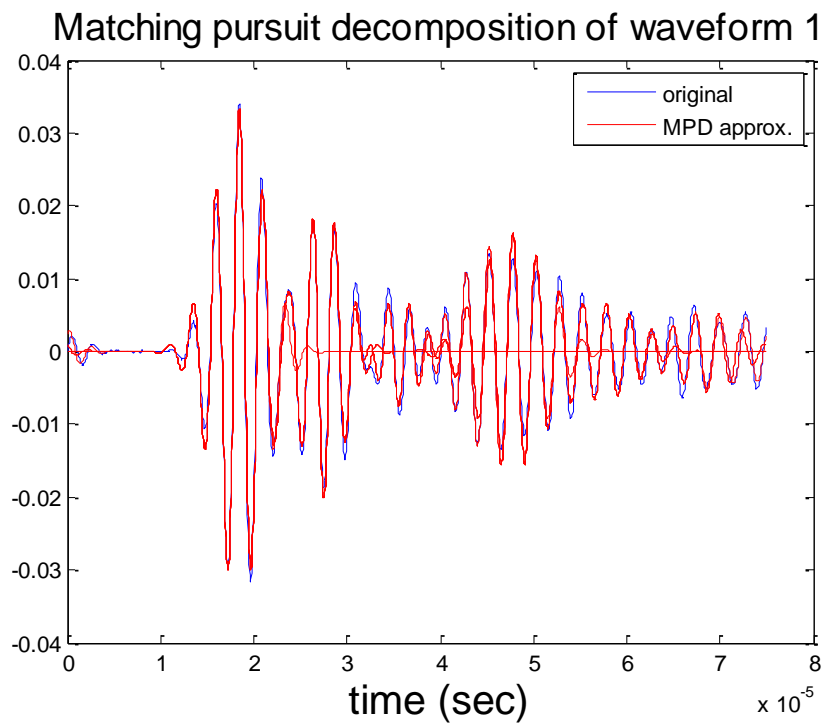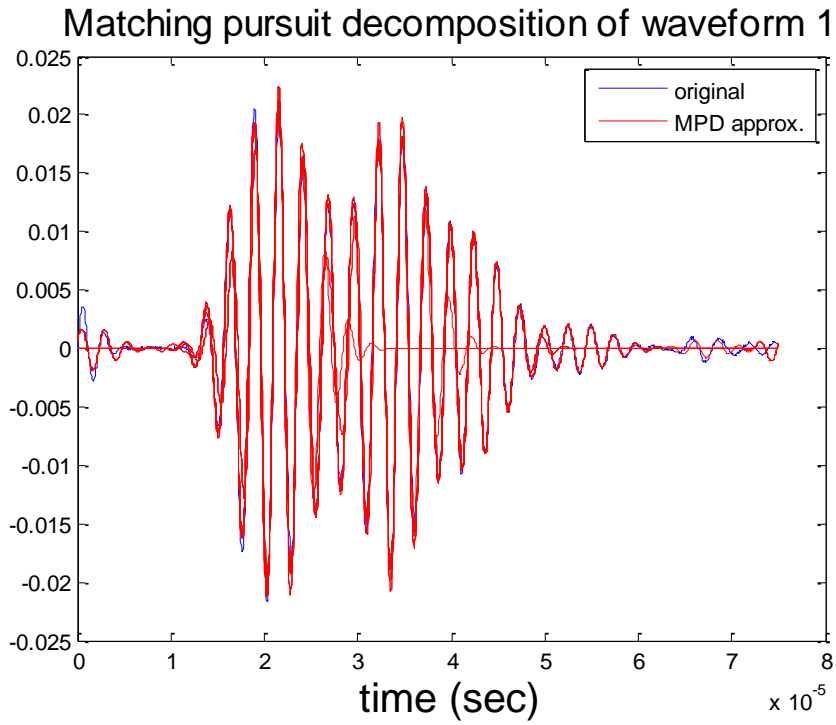
Figure 21. Change in signal for Panel A (PZT A to C) from 30 ^{o}C (top) to

70 ^{o}C (bottom)

Table 1. Wave times for Panel A and B (x10-4 sec.). NF = Not Found

	Temp C	S_0	S'_{01}	S'_{02}	MC	A_0
A		0.184	0.2735	0.345	NA	0.476
B	20	0.2005	0.301	0.444	0.539	0.6465
		0.1845	0.275	0.355	NA	0.478
	30	0.2	0.301	0.4565	0.5415	0.6605
		0.185	0.276	0.36	NA	0.48
	40	0.2115	0.302	0.4595	0.558	0.6755
		0.1855	0.29	0.362	NA	0.48
	50	0.212	0.3035	0.4635	0.564	0.7055
		0.2005	0.3185	0.407	NA	0.505
	60	0.2155	0.309	0.4825	0.561	**NF**
		0.2115	0.335	0.4235	NA	0.5245
	70	0.2155	0.309	0.5015	0.5605	**NF**
		0.218	0.3385	0.424	NA	0.544
	80	0.2155	0.309	0.5015	0.5605	**NF**

These results show that even as temperature changes, the mode conversion can still be detected for higher temperatures until the dispersion and attenuation caused by the thermal effects on the material properties of the panels masks the converted mode and the A_0 mode. Temperatures beyond 80°C caused the PZT adhesive to partially fail as well so as to be able to discover some, but not all of the modes. These effects can be seen in Figure 22. The MPD algorithm was still

able to uncover the majority of the modes. Further analysis of the data shows that the trend in ToF shifts is mostly linear. Figure 23 shows this for the second S_0 reflection, S'_{02}. Similar results as presented in Table 1 were found for the data collected from PZT B and D. Because the trend is linear, baseline data collected at one temperature can be compared to damaged data collected from a separate panel at a different temperature by stretching the signal according to the slope of the trend. This displays the robustness of the system to be applied in industry where systems are needed that can withstand the variability of real world application.
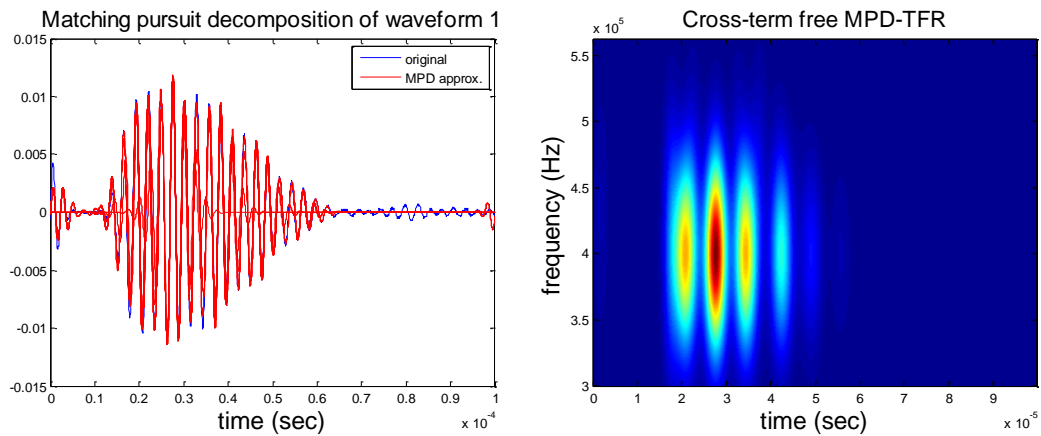
Figure 22. Panel A at 90 ^{o}C. TFR reveals data otherwise masked in time domain
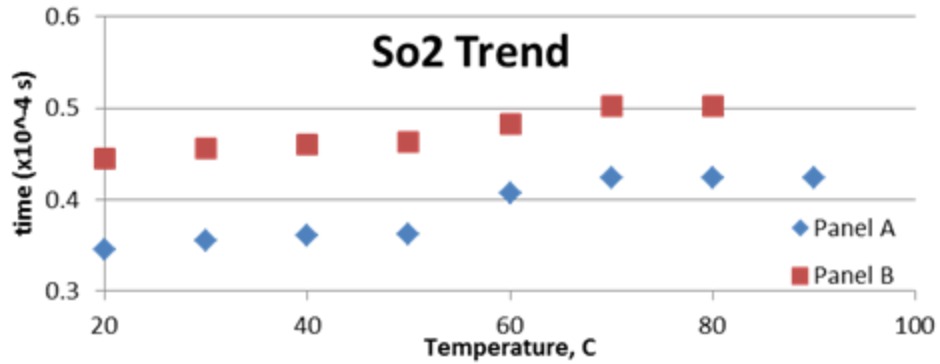
Figure 23. Trend for ToF change in S'$_{02}$ for Panels A and B

3.3   Concluding Remarks

In this work, the detection of damage in a stiffened composite panel under varying temperature using mode conversion was investigated. The effect of geometric variability is investigated by using two separate panels representing healthy and damaged states. Data was collected from the two panels using three piezoelectric sensors at temperature ranging from 20°C to 80°C in 10°C increments. Arrival times for the fundamental modes, their reflections, and mode conversions were identified and recorded using the Matching Pursuit Decomposition algorithm. By using wave propagation analysis, the reflected mode corresponding to damage was identified and the existence of delamination was shown. Results from this work show that the damage feature in the data is not only extractable at higher temperatures, but, due to the linearity of shifting in the ToF of the modes, that the data from one panel at one temperature can be directly compared to another panel at another temperature for baseline comparison.

CHAPTER 4

CONCLUDING REMARKS AND DISCUSSION OF FUTURE WORK

There is increased demand for robust and efficient Structural Health Monitoring (SHM) techniques for use in Condition Based Monitoring. *In situ* systems that are capable of detecting the early signs of damage in exposed and unexposed structural elements offer a solution to this problem. Robust systems will help reduce the number of inspections and provide better useful life estimates. These systems require the development of different sensing technologies, algorithms, and procedures to detect, localize, quantify, and characterize damage in aerospace structures so that strong estimations in the remaining useful life can be determined.

The research presented in this paper describes a methodology based on the use of piezoelectric transducers and guided Lamb waves. It investigates the ability of Lamb waves to detect damage in feature dense anisotropic composite panels, unlike much of the current research that negates the effects of experimental variability. Experiments were first conducted on a single blade-stiffened anisotropic composite panel to localize delamination damage caused by impact. A computationally efficient correlative approach using the energy of the converted mode as the damage index was used to detect and localize the damage. The advantage of this was utilizing a simplistic means to determine the existence and location of damage without having to do a more complex wave propagation analysis or having to take into account the geometric complexities of the test specimen as is required in ToF approaches. The damage features were

successfully extracted and the location of the damage was estimated with a satisfactory amount of accuracy. A higher number of sensors in the network would increase accuracy, but it would also add to the computational expense.

Next, the effects of temperature and experimental variability on damage detection were investigated. This was done by testing two separate panels, one healthy, one damaged, and seeing if mode conversions could be revealed at varying temperatures while using benchmark comparisons from separate test specimens. Results from this work show that the damage feature in the data is not only extractable at higher temperatures, but, due to the linearity of shifting in the ToF of the modes, the data from one panel at one temperature can be directly compared to another panel at another temperature for baseline comparison due to linearity of the collected data.

Further research based on this work should be conducted on feature dense anisotropic panels using mode conversion as a means for not only detecting and localizing damage, but also for quantifying and characterizing the damage. There is evidence from this research suggesting the energy of the converted mode is higher when the sensor path is closer to the damage and when the size of the damage changes. Further study on this subject could lead to a method for calculating the size of damage based on the research in this paper. Information linking the energy of the converted modes to their ToF could reveal a way to predict the size of the damage. Future work should also include a study into the effects of damage type on the energy and temporal information contained in the converted modes. In addition this research is also warranted because it studies the

sensitivity of the converted mode to other kinds of variability other than temperature, such as varying sensor placement on fiber paths, effects of varying volume fraction in composites, and subtle thickness changes.

REFERENCES

[1]   Yu, Y.-H., Choi, J.-H., Kweon J.-H., et al., "A study on the failure detection of composite materials using an acoustic emission," *Composite Structures*, Vol. 75, pp. 163–169, 2006.

[2]   Genest, M., Martinez, M., Mrad, N., et al., "Pulsed thermography for non-destructive evaluation and damage growth monitoring of bonded repairs," *Composite Structures*, Vol. 88, pp. 112-120, 2009.

[3]   Şimşir, M., and Ankara, A., "Comparison of two non-destructive inspection techniques on the basis of sensitivity and reliability," *Materials & Design*, Vol. 28, pp. 1433-1439, 2007.

[4]   Aymerich, F., and Meili, S., "Ultrasonic evaluation of matrix damage in impacted composite laminates," *Composites Part B: Engineering*, Vol. 31, pp. 1-6, 2000.

[5]   Farrar, C. R., Park, G., Allen, D. W., and Todd, M.D., "Sensor Network Paradigms for Structural Health Monitoring," *Struct. Control and Health Monit.*, Vol. 13, pp. 210-225, 2006.

[6]   Soni, S., Das, S., and Chattopadhyay, A., "Simulation of Damage Features in a Lug Joint using Guided Waves," *Journal of Intelligent Materials Systems and Structures*, Vol. 20, pp. 1451-1464, 2009.

[7]   Soni, S., Das, S., and Chattopadhyay, A., "Optimal Sensor Placement for Damage Detection in Complex Structures," *Proceedings of the ASME 2009 Conference on Smart Materials, Adaptive Structures and Intelligent Systems*, 2009.

[8]   Coelho, C. K., Das, S., and Chattopadhyay, A., "A hierarchical classification scheme for computationally efficient damage classification," *Proc. IMechE, Part G: J. Aerospace Engineering*, Vol. 223, pp. 497-505, 2009.

[9]   Pearson, J.D., Zikry, M.A., Prabhugoud, M., and Peters, K., "Global-local Assessment of Low-velocity Impact Damage in Woven Composites", *Comp. Mat.*, Vol. 41, pp. 2759-2783, 2007.

[10]   Coelho, C. K., Das, S., Chattopadhyay A., et al., "Detection of fatigue cracks and torque loss in bolted joints," *Proceedings of SPIE*, vol. 6532, no. 653204-12, 2007.

[11] Matt, H.M., and di Scalea, F.L, "Macro-fiber composite piezoelectric rosettes for acoustic source location in complex structures," *Smart Mater. Struct.,* Vol. 16, pp. 1489-1499, 2007.

[12] Betz, D., Thursby, G., Culshaw, B. and Staszewski, W., "Structural Damage Location with Fiber Bragg Grating Rosettes and Lamb Waves," *Structural Health Monitoring*, Vol. 6, pp. 299-308, 2007.

[13] Soni, S., Kim, S. B., and Chattopadhyay, A., "Reference Free Fatigue Crack Detection, Localization and Quantification in Lug Joints," *51st AIAA/ASME/ASCE/AHS/ASC Structures, Structural Dynamics, and Materials Conference*, 2010.

[14] Kim, S. B., and Sohn, H., "Instantaneous reference-free crack detection based on polarization characteristics of piezoelectric materials," *Smart Mat. and Struct.*, Vol. 16, pp. 2375-2387, 2007.

[15] Liu, Y., Fard, M., Kim, S.B., Chattopadhyay, A., Doyle, D., "Structural health monitoring and damage detection in composite panels with multiple stiffeners," *52th AIAA/ASME/ASCE/AHS/ASC Structures, Structural Dynamics, and Materials Conference* , AIAA-2011-1859, 2011.

[16] Su, Z., Ye, L., Lu, Y., "Guided Lamb waves for identification of damage in composite structures: A review," *J. Sound and Vibration*, Vol. 295, pp. 753-780, 2006.

[17] M.J.S. Lowe, "Matrix techniques for modelling ultrasonic waves in multilayered media," *IEEE Transactions on Ultrasonics, Ferroelectrics and Frequency Control*, Vol. 42, pp. 525–542, 1995.

[18] D.E. Chimenti, "Guided waves in plates and their use in materials characterization," *Applied Mechanics Reviews*, Vol. 50, pp. 247–284, 1997.

[19] D.C. Worlton, "Experimental confirmation of Lamb waves at megacycle frequencies," *Journal of Applied Physics*, Vol. 32, pp. 967–971, 2006.

[20] J.D. Achenbach, "Wave Propagation in Elastic Solids," *North-Holland Publishing Company*, Amsterdam, 1973.

[21] Lu, Y., et al., "Time-Domain Analyses and Correlations of Lamb Wave Signals for Damage Detection in a Composite Panel of Multiple Stiffeners," *J. Composite Materials*, Vol. 43, pp. 3211-3230, 2009.

[22]   Wang, D., et al., "Probability of the Presence of Damage Estimated from an Active Sensor Network in a Composite Panel of Multiple Stiffeners," *Composites Science and Technology*, Vol. 69, pp. 2054-2063, 2009.

[23]   Michaels, J.E., "Detection, Localization and Characterization of Damage in Plates with an In Situ Array of Spatially Distributed Ultrasonic Sensors," *Smart Materials and Structures*, Vol. 17, pp. 1726-1741, 2008.

[24]   Lu, Y., Ye, L., and Su, Z., "Crack Identification in Aluminum Plates using Lamb Wave Signals of a PZT Sensor Network," *Smart Materials and Structures*, Vol. 15, pp. 839-849, 2006.

[25]   Sohn, H., et al., "Wavelet-Based Active Sensing for Delamination Detection in Composite Structures," *Smart Materials and Structures*, Vol. 13, pp. 153-160, 2004.

[26]   Su, Z., Ye, L., and Bu, X., "A Damage Identification Technique for CF/EP Composite Laminates Using Distributed Piezoelectric Transducers," *Composite Structures*, Vol. 57, pp. 465-471, 2002.

[27]   Lu, Y., and Michaels, J.E., "A Methodology for Structural Health Monitoring with Diffuse Ultrasonic Waves in the Presence of Temperature Variations," *Ultrasonics*, Vol. 43, pp. 717-731, 2005

[28]   Zhao, X., Gao, H., Zhang, G., Ayhan, B., Yan, F., Kwan, C., Rose, J.L., "Active health monitoring of an aircraft wing with embedded piezoelectric sensor/actuator network: I. Defect detection, localization and growth monitoring," Smart Mater. Struct., 16, pp. 1208-1217, 2007.

[29]   Das, S., Kyriakides, I., Chattopadhyay, A., Papandreou-Suppappola, A., "Monte Carlo Matching Pursuit Decomposition Method for Damage Quantification in Composite Structures", *Journal of Intelligent Material System and Structures*, Vol. 20, pp. 647-658, 2009.

[30]   Kess, H.R., and Adams, D.E., "Investigation of Operational and Environmental Variability Effects on Damage Detection Algorithms in a Woven Composite Plate," *Mech. Sys. Sig. Process.*, Vol. 21, pp. 2394-2405, 2007.

[31]   Yekani Fard, M., Chattopadhyay, A., and Liu, Y., (2012). "Multi-linear stress-strain and closed-form moment curvature response of epoxy resin materials," *International Journal of Mechanical Sciences*, doi: 10.1016/j.ijmecsci.2012.01.009,

[32]   Yekani Fard, M., Liu, Y., and Chattopadhyay, A., (2012) "Characterization of Epoxy Resin Including Strain Rate Effects Using Digital Image Correlation System," *Journal of Aerospace Engineering*, doi:10.1061/(ASCE)AS.1943-5525.0000127,

[33]   Yekani Fard, M., Liu, Y., and Chattopadhyay, A., (2012) "Analytical Solution for Flexural Response of Epoxy Resin Materials," *Journal of Aerospace Engineering*, doi: 10.1061/(ASCE)AS.1943-5525.0000133

[34]   Yekani Fard, M., Chattopadhyay, A., and Liu, Y. "Influence of Load Type and Stress Gradient on Flexural Strength of an Epoxy Resin Polymeric Material," *Journal of Aerospace Engineering*, 2012, 10.1061/(ASCE)AS.1943-5525.0000228

[35]   Lu, Y., and Michaels, J.E., "A Methodology for Structural Health Monitoring with Diffuse Ultrasonic Waves in the Presence of Temperature Variations," *Ultrasonics*, Vol. 43, pp. 717-731, 2005.

[36]   Di Scalea, F.L., Salamone, S., "Temperature Effects in Ultrasonic Lamb Wave Structural Health Monitoring Systems," *J. Acoust. Soc. Am.*, Vol. 124, pp. 161-174, 2008.

[37]   Salamone, S., et al., "Guided-Wave Health Monitoring of Aircraft Composite Panels under Changing Temperature," *J. Intel. Mat. Sys. And Struc.*, Vol. 20, pp. 1079-1090, 2009.

[38]   Croxford, A.J., et al., "Efficient Temperature Compensation Strategies for Guided Wave Structural Health Monitoring," *Ultrasonics*, Vol. 50, pp. 517-528, 2010.

[39]   Michaels, T.E., and Michaels, J.E., "Sparse Ultrasonic Transducer Array for Structural Health Monitoring," *Review of Progress in Quantitative Nondestructive Evaluation,* Vol. 23b, pp. 1468-1475, 2004.

[40]   Gao, H., Shi, Y., and Rose, J.L., "Guided Wave Tomography on an Aircraft Wing with Leave In Place Sensors," *Review of Progress in Quantitative Nondestructive Evaluation,* Vol. 24b, pp. 1788-1794, 2005.

[41]   S.H.D. Valdes, C. Soutis, "A structural health monitoring system for laminated composites," *Proceedings of DETC*, Pittsburgh, PA, USA, pp. 2013–2021, 2007.

[42]   H. Sohn, C.R. Farrar, "Damage diagnosis using time series analysis of vibration signals," *Smart Materials and Structures*, Vol. 10, pp 446-451, 2001.

[43]   C. Zang, M.I. Friswell, M. Imregun, "Structural damage detection using independent component analysis," *Structural Health Monitoring: An International Journal*, Vol. 3, pp. 69–83, 2004.

[44]   M. Veidt, T. Liu, S. Kitipornchai, "Modelling of Lamb waves in composite laminated plates excited by interdigital transducers," *NDT & E International*, Vol. 35, pp. 437–447, 2002.

[45]   Y.L. Koh, W.K. Chiu, N. Rajic, "Effects of local stiffness changes and delamination on Lamb wave transmission using surfacemounted piezoelectric transducers," *Composite Structures*, Vol. 57, pp. 437–443, 2002.

[46]   K. Heller, L.J. Jacobs, J. Qu, "Characterization of adhesive bond properties using Lamb waves," *NDT & E International*, Vol. 33, pp. 555–563, 2000.

[47]   F. EI Youbi, S. Grondel, J. Assaad, "Signal processing for damage detection using two different array transducers," *Ultrasonics*, Vol. 42, pp. 803–806, 2004.

[48]   D. Gabor, "Theory of Communication," *J. IEEE,* Vol. 93, pp. 429-457, 1946.

[49]   Z. Hou, M. Noori, R.S. Amand, "Wavelet-based approach for structural damage detection," *Journal of Engineering Mechanics*, Vol. 126, pp. 677–683, 2000.

[50]   M. Lemistre, D.L. Balageas, "Structural health monitoring system based on diffracted Lamb wave analysis by multiresolution processing," *Smart Materials and Structures*, Vol. 10, pp. 504–511, 2001.

[51]   S.S. Kessler, S.M. Spearing, C. Soutis, "Damage detection in composite materials using Lamb wave methods," *Smart Materials and Structures*, Vol. 11, pp. 269–278, 2002.

[52]   Mallat, S.G., and Zhang, Z., "Matching Pursuits with Time-Frequency Dictionaries," *IEEE Transactions on Signal Processing,* Vol. 41, pp. 3397-3412, 1993.

[53]   Chakraborty, D., Kovvali, N., Wei, J., Papandreou-Suppappola, A., Cochran, D., and Chattopadhyay, A., "Damage Classification Structural Health Monitoring in Bolted Structures Using Time-Frequency Techniques", *Journal of Intelligent Material System and Structures*, Vol. 20, pp. 1289–1305, 2009.

[54]   C.H. Wang, J.T. Rose, F.-K. Chang, "A synthetic time-reversal imaging method for structural health monitoring," *Smart Materials and Structures*, Vol. 13, pp. 415–423, 2004.

[55]   Park, H.W., Sohn, H., Kincho, H.L., and Farrar, C.R., "Time Reversal Active Sensing for Health Monitoring of a Composite Plate," *J. Sound and Vib.,* Vol. 302, pp. 50-66, 2007.

APPENDIX A

MPD CODE

```matlab
% Matching Pursuit Decomposition based on Gaussian Atom Time-
Frequency Dictionary

% clear;
pack; close all; clc;

% Initialize parameters
N =1800;                          % Number of samples
delt = 1/(2e7);                    % Time step
Nf = 15;                          % Number of f for dictionary
fmin = 400e3;                      % Minimum f for dictionary
fmax = 450e3;                      % Maximum f for dictionary
Na = 300;                         % Number of a for dictionary
amin = 2.0e5;   % Minimum a for dictionary (controls max width of
atom)
amax = 3.5e5;   % Maximum a for dictionary (controls max width of
atom)
Nw = 1;                           % Number of waveforms
Niter = 10;                       % Number of MP iterations
Nd = Na*Nf;                       % Number of dictionary elements
excluding time-shifts (including time-shifts, total number is
Na*Nf*N)

% Pre-allocate memor2
fprintf(1,'Pre-allocating memory...');
tmp_vec3 = zeros(Nd,1);
tmp_vec4 = zeros(Nd,1,'int32');
mp_dict = zeros(N,Nd);
coeff_mp = zeros(Niter,Nw);
tau_mp = zeros(Niter,Nw,'int32');
a_mp = zeros(Niter,Nw,'int32');
f_mp = zeros(Niter,Nw,'int32');
fprintf(1,'done.\n');

% Create dictionary and compute its FFT
fprintf(1,'Creating dictionary and computing its FFT...');
Nb2 = N/2;
t = [-Nb2:Nb2-1]'*delt;
t2 = t.^2;
TWO_PI = pi+pi;
fstep = (fmax-fmin)/(Nf-1);
omega = TWO_PI*(fmin+[0:Nf-1]*fstep);
count = 1;
astep = (amax/amin)^(1/(Na-1));
a = amin;
for i = 1 : Na,
    a2 = a*a;
    for j = 1 : Nf,
        % Gaussian atom
        mp_dict(1:N,count) = exp(-t2*a2).*cos(omega(j)*t);
        % Normalize
        mp_dict(1:N,count) =
mp_dict(1:N,count)/norm(mp_dict(1:N,count),2);
        count = count+1;
    end
```

```matlab
        a = a*astep;
    end
    % Symmetric dictionary elements => no flipping required
    mp_dict_hat = fft(mp_dict);
    fprintf(1,'done.\n');

    % Generate signal(s): Nw waveforms stored columnwise in the
    variable `data'
    fprintf(1,'Generating signal(s)...');
    cd('C:\Users\Anthony\Documents\aerospace\MastersResearch\SPIE2012
    \SPIETemp\CP50');  % File Path containing data

    path1=load('burst_5M_4_5cycles_400k_A3_1'); % file name

    path=path1(:,6); % data column in file
    ai=20001;           % data start point
    af=ai+N-1;
    data = path(ai:af);
    store_data = data;
    fprintf(1,'done.\n');

    % Compute matching pursuit decomposition
    fprintf(1,'Computing matching pursuit decomposition...\n');
    for i = 1 : Nw,
        fprintf(1,'Waveform %d:\n',i);
        for j = 1 : Niter,
            % FFT the residual
            tmp_vec1 = fft(data(1:N,i));
            for k = 1 : Nd,
                % Multiply with FFT of dictionary element and IFFT
                tmp_vec2 = ifft(mp_dict_hat(1:N,k).*tmp_vec1);
                [tmp,tmp_vec4(k)] = max(abs(tmp_vec2));
                tmp_vec3(k) = tmp_vec2(tmp_vec4(k));
            end
            [tmp,ind] = max(abs(tmp_vec3));
            coeff_mp(j,i) = tmp_vec3(ind);
            tau_mp(j,i) = tmp_vec4(ind)-1;
            tmp = rem(ind-1,Nf);
            a_mp(j,i) = (ind-1-tmp)/Nf+1;
            f_mp(j,i) = tmp+1;
            % Residual
            data(1:N,i) = data(1:N,i) - coeff_mp(j,i)*[mp_dict(N-
    tmp_vec4(ind)+2:end,ind); mp_dict(1:N-tmp_vec4(ind)+1,ind)];
            fprintf(1,'...iteration %d complete\n',j);
        end
    end
    fprintf(1,'Done.\n');

    % Waveform for which to plot matching pursuit decomposition
    result (1 <= w <= Nw)
    w = 1;

    % a, f, and tau
    astep = (amax/amin)^(1/(Na-1));
```

```matlab
a = amin*(astep.^[0:Na-1]');
a_mp = a(a_mp);
fstep = (fmax-fmin)/(Nf-1);
f = [fmin:fstep:fmax]';
f_mp = f(f_mp);
tau_mp = double(tau_mp);

% Plot matching pursuit decomposition results
f = zeros(N,1);
data = store_data;
figure, plot(t+N/2*delt,data);
iter = [1:Niter];
e = zeros(1,Niter);
for j = iter,
    g = exp(-a_mp(j,w)^2*t.^2).*cos(2*pi*f_mp(j,w)*t);
    g = g/norm(g);
    g = [g(N-tau_mp(j,w)+1:N); g(1:N-tau_mp(j,w))];
    f = f + coeff_mp(j,w)*g;
    e(j) = (norm(f-data)/norm(data))^2;
    hold on, plot(t+N/2*delt,f,'r');
    pause
end

title(['Matching pursuit decomposition of waveform ' num2str(w)
],'FontSize',16); xlabel('time (sec)','FontSize',18);
legend('original','MPD approx.');
figure, plot([0 iter],[1 e],'-o');
title('Residual signal energy fraction','FontSize',18);
xlabel('MPD iteration no.','FontSize',18);

% MPD-TFR
fmin_tfr = fmin*0.75;
delf_tfr = fstep/20;
fmax_tfr = fmax*1.25;
fvec = [fmin_tfr:delf_tfr:fmax_tfr];
ind = find(tau_mp>N/2); tau_mp(ind) = tau_mp(ind)-N; % compensate
shifts
[X,Y] = meshgrid(t,fvec);
Z = single(zeros(length(fvec),N));
for j = iter,
    Z = Z + coeff_mp(j,w)^2*exp(-(2*a_mp(j,w)^2)*(X-
tau_mp(j,w)*delt).^2 - 4*pi^2*(Y-f_mp(j,w)).^2/(2*a_mp(j,w)^2));
% Z is the outpout data set that is plotted for the scalogram
end
figure, imagesc(t+N/2*delt,fvec,Z);
axis xy;
axis tight;
xlabel('time (sec)','FontSize',18);
ylabel('frequency (Hz)','FontSize',18);
title('Cross-term free MPD-TFR','FontSize',16);

%% time of arrival in spectrogram
t_spec = tau_mp*delt+(N/2)*delt;

%% Actual time of arrival of the waves
```

```
t_act = t_spec
```

APPENDIX B

MAXIMUM NORMALIZED ENERGY COMPARISON CODE

```matlab
close all; clc;

%run MPD code twice and set H = Z for healthy data
%and D = Z for damaged data
H = max(H)/max(max(H)) %sets H equal to maxium energy in the
frequency
                        %for each point in the time domain and
normalizes it
                        %by the maximum energy in the plot
D = max(D)/max(max(D)) %same as before but for the damaged data
set

figure
plot(1:N,H)             %N comes from the MPD code and is the
sample size
hold on
plot(1:N,D,'r')

%from this plot, the new mode as a result of damage will appear,
and using
%the trace function, the normalized energy at this point can be
found
```

APPENDIX C

TOMOGRAPHICAL LOCALIZATION CODE

```
clc
clear all
close all


%this is the set of Damage indexes found from MPD and maximum
normalized energy method. Each space in the matrix is paired to
its relative sensor path in K1234, i.e., the first spot in AD1 is
sensor path 1-4, spot 2 is path 1-5, etc. must fill this matrix
in manually
AD1 =
[0;0;0;0;0;0;0;0;0.1419;0;0;0;0.2293;0;0;0;0;0;0.6671;0;0;0;0;0;.
1869;0.9015;0;0;0;0.6376;0.7739;0.3168;0;0;0;0.6376;0;0.2293;0;0.
1869;0.7739;0.1419;0.6671;0.9015;0.3168];

%This is the matrix that contains all sensor paths used
K=[1 4;1 5;1 6;1 8;2 4;2 5;2 6;2 7;2 9;3 4;3 5;3 6;3 8;4 1;4 2;4
3;4 7;4 8;4 9;5 1;5 2;5 3;5 7;5 8;5 9;6 1;6 2;6 3;6 7;6 8;6 9;7
2;7 4;7 5;7 6;8 1;8 3;8 4;8 5;8 6;9 2;9 4;9 5;9 6];

%define sensor/actuator locations (in mm)
P=[0 0;0 10;0 20;10 0;10 10;10 20;20 0;20 10;20 20];
%sensor order 1, 2, 3, 4, 5, 6, 7, 8, 9

%Determine D.k (sensor path lengths)
for i = 1:44
    P1=K(i,1);
    P2=K(i,2);
    DK(1,i)=sqrt((P(P2,1)-P(P1,1))^2+(P(P2,2)-P(P1,2))^2);
end

%create grid / define number of points this controls the number
of points used in the tomographical search. More points means
more time
num=100;
x=(0:num)*20/num;
y=(0:num)*20/num;

%define beta
B=1.05;

for i = 1:length(x)
    for j = 1:length(y)
        for z = 1:length(AD1)
            kval=z;
            xval=x(i);
            yval=y(j);
            %define actuator location and distance from grid
point
            Ax=P(K(z,1),1);
            Ay=P(K(z,1),2);
            Dak=sqrt((x(i)-Ax)^2+(y(j)-Ay)^2);
            %define sensor location and distance from grid point
            Sx=P(K(z,2),1);
```

69

```matlab
            Sy=P(K(z,2),2);
            Dsk=sqrt((x(i)-Sx)^2+(y(j)-Sy)^2);
            %solve for R (relative distance from grid point to
sensor path)
            R(i,j,z)=(Dak+Dsk)/DK(1,z)-1;
            %solve for W
            if (R(i,j,z) < B)
                W(i,j,z)= 1-R(i,j,z)/B;
            elseif (R(i,j,z) >= B)
                W(i,j,z)=0;
            end

            % solve for P(x,y) related to each sensor path
(probability of damage at the grid point)
            Prob(z)=AD1(z)*W(i,j,z);

            %remove probability for points that lie on a PZT
            if (Ax == xval) && (Ay == yval)
                Prob(z)=0;
            end
            if (Sx == xval) && (Sy == yval)
                Prob(z)=0;
            end
        end
        %find total probability of damage at grid point (x,y)
        PROB(i,j)=sum(Prob);
    end
end



PROBmax = max(max(PROB));

%normalize probability
PROB=PROB/max(max(PROB));

%determine max probability point(s)
[ROW,COL]=find(PROB==1);

%plot results
%scalogram of probability density
figure
imagesc(x,y,PROB')
hold on
plot(14,16,'+','MarkerSize',20,'LineWidth',2)
hold on
plot(x(ROW),y(COL),'+r','MarkerSize',10,'LineWidth',3)
hold on
plot(P(:,1),P(:,2),'+')
axis([-1 21 -1 21])
xlabel('x-axis (cm)')
ylabel('y-axis (cm)')
title('damage localization')
```

```matlab
%lines showing probability of damage
figure
[C,h] = contour(x,y,PROB',[.9,.95,.98,.99,1]);
clabel(C,h)
hold on
plot(14,16,'+','MarkerSize',20,'LineWidth',2)
hold on
plot(x(ROW),y(COL),'+r','MarkerSize',10,'LineWidth',3)
hold on
plot(P(:,1),P(:,2),'+')
axis([-1 21 -1 21])
xlabel('x-axis (cm)')
ylabel('y-axis (cm)')
title('damage localization')
```